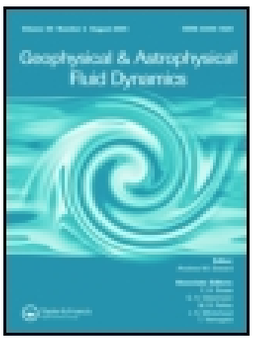

Taylor & Francis
Taylor & Francis Group

Geophysical & Astrophysical Fluid Dynamics

ISSN: 0309-1929 (Print) 1029-0419 (Online) Journal homepage: http://www.tandfonline.com/loi/ggaf20

Rotating magnetic shallow water waves and instabilities in a sphere

X. Márquez-Artavia, C. A. Jones & S. M. Tobias

To cite this article: X. Márquez-Artavia, C. A. Jones & S. M. Tobias (2017): Rotating magnetic shallow water waves and instabilities in a sphere, Geophysical & Astrophysical Fluid Dynamics, DOI: 10.1080/03091929.2017.1301937

To link to this article: http://dx.doi.org/10.1080/03091929.2017.1301937

Published online: 27 Mar 2017.

GEOPHYSICAL AND ASTROPHYSICAL FLUID DYNAMICS, 2017
http://dx.doi.org/10.1080/03091929.2017.1301937

Taylor & Francis
Taylor & Francis Group

Rotating magnetic shallow water waves and instabilities in a sphere

X. Márquez-Artavia, C. A. Jones and S. M. Tobias

School of Mathematics, University of Leeds, Leeds, UK

ABSTRACT

Waves in a thin layer on a rotating sphere are studied. The effect of a toroidal magnetic field is considered, using the shallow water ideal MHD equations. The work is motivated by suggestions that there is a stably stratified layer below the Earth's core mantle boundary, and the existence of stable layers in stellar tachoclines. With an azimuthal background field known as the Malkus field, $B_\phi = B_0 sin\theta$, θ being the co-latitude, a non-diffusive instability is found with azimuthal wavenumber $m = 1$. A necessary condition for instability is that the Alfvén speed exceeds $\Omega_0 R_0$ where Ω_0 is the rotation rate and R_0 the sphere radius. Magneto-inertial gravity waves propagating westward and eastward occur, and become equatorially trapped when the field is strong. Magneto-Kelvin waves propagate eastward at low field strength, but a new westward propagating Kelvin wave is found when the field is strong. Fast magnetic Rossby waves travel westward, whilst the slow magnetic Rossby waves generally travel eastward, except for some $m = 1$ modes at large field strength. An exceptional very slow westward $m = 1$ magnetic Rossby wave mode occurs at all field strengths. The current-driven instability occurs for $m = 1$ when the slow and fast magnetic Rossby waves interact. With strong field the magnetic Rossby waves become trapped at the pole. An asymptotic analysis giving the wave speed and wave form in terms of elementary functions is possible both in polar trapped and equatorially trapped cases.

ARTICLE HISTORY
Received 22 September 2016
Accepted 28 February 2017

KEYWORDS
MHD waves; shallow water model; azimuthal field; rotating MHD fluids

1. Introduction

Waves are ubiquitous in geophysical and astrophysical fluids. For many such systems the interaction of rotation and stratification leads naturally to the propagation of wave modes at a wide range of frequencies. Waves are known to play an important role in neutral fluids such as the Earth's ocean and atmosphere with inertial waves (and near-inertial waves) believed to play a role in transport, mixing and dissipation in the ocean, whilst gravity waves are vital in transferring energy, momentum and species between different atmospheric layers and also influence upper atmosphere winds, turbulence, temperature and chemistry in Earth's oceans and atmosphere (see e.g. Vallis 2006). Global scale planetary waves such as Rossby waves are known to have an influence on terrestrial weather and potentially climate and have been implicated in playing a potential role in generating mean zonal

CONTACT X. Márquez-Artavia mmxmm@leeds.ac.uk

flows on gas giants such as Jupiter and Saturn (see e.g. Grazzini and Vitart 2015, Legarreta *et al.* 2016).

For electrically conducting fluids in geophysics and astrophysics the magnetic field will strongly influence the wave dynamics. Though rotating magnetohydrodynamic waves can be important in convectively unstable environments, their role is complicated owing to the presence of turbulence. In stably stratified environments these waves can play a similar role in transport and driving to their hydrodynamic counterparts.

Rotating MHD waves have been extensively studied in the context of the Earth's fluid outer core, which is believed to be the seat of the geodynamo. Following early work by Hide Hide (1969) and Acheson and Hide (1973) there have been many investigations (see e.g. Finlay *et al.* 2010). Of particular interest for the current investigation is the proposed presence of a stably stratified layer at the Core-Mantle Boundary (CMB). This layer was theoretically predicted by Braginsky (1998), who discussed the nature of some of the waves that might be found in such a layer. In particular, he established that the existence of this stable stratified layer a the top of the core would permit the propagation of magnetic Rossby waves and suggested that this oscillation might be related to short time-scale geomagnetic secular variation, length of day variation and oscillation of the pole position. Interestingly, there is now significant observational evidence that such a layer exists. Analysing seismic velocities profiles, Helffrich and Kaneshima (2010), observed a reduction in wave speeds just below the CMB of the Earth; these differences suggest the presence of a stably stratified layer of about 300 km in thickness at the top of the core.

The presence of wave-modes in the stably stratified interior of the Sun has also recently received renewed attention. The solar tachocline is a thin layer of strong radial and latitudinal differential rotation at the base of the solar convection zone that has been revealed by helioseismology (see e.g. Spiegel and Zahn 1992, Tobias 2015, Miesch 2005, Christensen-Dalsgaard andThompson 2007). The tachocline is believed to play an important role in the generation of the eleven year activity cycle through dynamo action. Theoretical investigation of the tachocline has shown that it is the potential seat of many MHD instabilities including magnetic buoyancy instabilities (Hughes 2007), double-diffusive shear instabilities (see e.g. Rashid *et al.* 2008) and joint instabilities of the differential rotation and toroidal magnetic field (which we shall discuss in more detail later) (Gilman and Fox 1997, Gilman and Dikpati 2002, Cally 2003, Cally *et al.* 2008, Hollerbach and Cally 2009). The presence and importance of wave motions has recently been emphasised by McIntosh and collaborators who have utilised 360° imaging observations to detect the presence of Rossby-like motions in the Sun's interior that are critical carriers of solar activity (Mcintosh *et al.* in press). Recent investigations of waves in the solar interior include those that focus on the interaction of internal gravity waves with magnetic fields, (see e.g. MacGregor and Rogers 2011, Mathis and de Brye 2011) in the radiative interior and those that look at local and global waves in the thin tachocline (Schecter *et al.* 2001, Zaqarashvili *et al.* 2007, Zaqarashvili *et al.* 2009, Heng and Spitkovsky 2009). These final investigations utilised the Shallow Water Magnetohydrodynamic equations (and model extensions thereof) introduced by Gilman (2000), which form the basis of this current investigation. A related strand of work is that of Sharif and Jones (2005) where the motion in the thin layer is assumed to be completely two-dimensional. This can be viewed as the limit of large buoyancy frequency in the shallow water system.

Final motivation for the study of waves in thin magnetised, stably stratified shells comes from the dynamics of atmospheres of exoplanets located close to their parent stars (sometimes called Hot Jupiters). It is possible that for these systems the ionosphere of the planet may extend downwards significantly into the atmosphere, making it necessary to include MHD effects into the stably stratified dynamics of these layers (Cho 2008, Koskinen *et al.* 2010, Koskinen *et al.* 2014).

In this paper we derive a description of the wave modes in a magnetised shallow water environment; there are three types of solutions: Magneto-Rossby waves, Magneto-Inertial gravity (MIG) waves and Kelvin modes. These oscillations are affected by rotation and the magnetic field through the parameters $\epsilon = 4\Omega_0^2 R_0^2/gH_0$ and $\alpha = v_A^2/4\Omega_0^2 R_0^2$. where Ω_0, H_0 and v_A are the rotation rate, the height of the layer and the Alfvén speed, respectively. The precise value of these non-dimensional parameters in any given astrophysical situation is uncertain and probably these can only be estimated to an order of magnitude. Moreover these parameters vary according to position. For example, the effective gravity in the layer varies significantly in the solar interior; in the tachocline there exist regions of high effective gravity (in the radiative layer) and lower effective gravity (in the overshoot region.) This will probably be the case for all stars with both a convecting layer and a stably stratified layer as the stratification must move from being essentially adiabatic in the convection layer to strongly subadiabatic in the stable layer. In the Earth, there is probably also a gradual transition from convection to stable stratification but this is difficult to characterise either theoretically or observationally via seismology. For this reason, rather than limiting attention on parameters believed to be relevant to either stellar or planetary interiors we give a full description of the wave modes in such systems as the parameters α and ϵ are varied, including many asymptotic limits, where the modes become trapped either at the poles or the equator. We also demonstrate how current-driven instabilities may arise through the interaction of two wave modes. Care should be taken in applying the results of the analysis here to any individual astrophysical object, owing both to the uncertainty in the correct parameters and to the simplified nature of the model presented here. The present work aims to describe the waves and instability types that can provide a guide to more realistic, but more complicated, models of particular objects where only numerical analysis is possible.

This paper is organised as follows. In Section 2, we present the MHD Shallow Water equations for a given toroidal magnetic field and linearise the system of equations. Solutions are developed as expansions of Associated Legendre polynomials, which are reduced to a set of eigenvalue matrix equations as detailed in Section 3. Section 4 is a summary of the hydrodynamic case, when the magnetic field is zero, which has been extensively studied by Longuet-Higgins (1968). In Section 5 we discuss the new numerical results in the magnetohydrodynamic case, and in Section 6 asymptotic theories are developed for cases when either the ϵ or α parameters are large and the waves are either equatorially or polar trapped. The conclusions are in Section 7.

2. Mathematical formulation of the problem

2.1. Shallow water equations in magnetohydrodynamics

The classical shallow water approximation of geophysical fluid dynamics, mentioned in the introduction above, can also be applied to a stratified layer of electrically conducting

fluid. Gilman (2000) established the shallow water MHD equations with a strong toroidal magnetic field,

$$\frac{\partial \boldsymbol{B}}{\partial t} + (\boldsymbol{u}\cdot\nabla)\boldsymbol{B} = (\boldsymbol{B}\cdot\nabla)\boldsymbol{u}, \tag{1a}$$

$$\frac{\partial \boldsymbol{u}}{\partial t} + (\boldsymbol{u}\cdot\nabla)\boldsymbol{u} + 2\boldsymbol{\Omega}\times\boldsymbol{u} = \frac{1}{\mu_0\rho}(\boldsymbol{B}\cdot\nabla)\boldsymbol{B} - g\nabla H, \tag{1b}$$

$$\frac{\partial H}{\partial t} + \nabla\cdot(H\boldsymbol{u}) = 0, \qquad \nabla\cdot(H\boldsymbol{B}) = 0. \tag{1c,d}$$

In these equations $\boldsymbol{u}$ and $\boldsymbol{B}$ represent the horizontal components of the velocity and magnetic field respectively. The operator ∇ is the horizontal gradient, ρ is the density of the fluid, μ_0 is the permeability of free space and H is the thickness of the layer.

There are a number of choices that need to be made to define a basic state on which the waves can propagate. Among these are the latitudinal profile for the magnetic field, height field, effective gravity, mean zonal flows and stresses on the layer from adjacent convecting layers. A range of mean profiles has been examined for both wave and instability problems in both the continuously stratified and shallow water models. For example, Tayler (1973, 1980) and Pitts and Tayler (1985) have considered the stability of magnetic fields in a continuously stratified layer where the force balance is maintained by imposing a position dependent gravity and pressure field. Within the hydrodynamic continuously stratified setting a basic state may be maintained via a latitudinal temperature gradient and a radial shear (often termed a thermal wind) (Rashid *et al.* 2008). Magnetohydrostatic balance may also be maintained by imposing a zonal jet in the stably stratified layer (Rempel *et al.* 2000). Within the confines of the shallow water MHD approximation a basic state may also be achieved by balancing the magnetic stress by an externally imposed stress that keeps the axisymmetric (average) part of the height field constant (Zaqarashvili *et al.* 2007) or by modifying the basic state height or effective gravity (Dikpati and Gilman 2001, Dikpati *et al.* 2003). All of these ingredients may be chosen in a plausible manner, though there is a great deal of latitude in the construction of the model.

For this reason we consider a simple model for which analytical progress may be made in asymptotic limits. We follow Zaqarashvili *et al.* (2007) in considering an unperturbed toroidal magnetic field

$$\boldsymbol{B} = B_\phi\hat{\boldsymbol{e}}_\phi,$$

and its perturbation is

$$\boldsymbol{b}' = b_\theta\hat{\boldsymbol{e}}_\theta + b_\phi\hat{\boldsymbol{e}}_\phi.$$

The velocity perturbation corresponds to

$$\boldsymbol{u} = u_\theta\hat{\boldsymbol{e}}_\theta + u_\phi\hat{\boldsymbol{e}}_\phi,$$

and the perturbed layer thickness is

$$H = H_0 + h,$$

where H_0 the basic state height is constant. We are therefore ignoring possible departures from sphericity of the constant pressure surfaces, and variations of H_0 with latitude, which

might be significant when the field is very strong. We note also that the imposition of a purely toroidal magnetic field requires the presence of an imposed current; in the Earth's core this current would connect to dynamo generated currents deep in the core and close in a thin diffusive layer near the CMB. In the tachocline case, currents associated with a strong belt of field in the tachocline might close in the radiative interior and the base of the convection zone. However, modelling these more complicated currents would greatly increase the complexity of the problem, and so they are not addressed here.

The linearised equations in spherical coordinates are, Zaqarashvili *et al.* (2007), but note a typographic error in their Equation (31),

$$\frac{\partial u_\theta}{\partial t} - 2\Omega_0 \cos\theta u_\phi + \frac{g}{R_0}\frac{\partial h}{\partial \theta} - \frac{B_\phi}{\mu_0 \rho R_0 \sin\theta}\frac{\partial b_\theta}{\partial \phi} + 2\frac{B_\phi}{\mu_0 \rho R_0}\frac{\cos\theta}{\sin\theta} b_\phi = 0, \tag{2a}$$

$$\frac{\partial u_\phi}{\partial t} + 2\Omega_0 \cos\theta u_\theta + \frac{g}{R_0 \sin\theta}\frac{\partial h}{\partial \phi} - \frac{b_\theta}{\mu_0 \rho R_0}\frac{\partial B_\phi}{\partial \theta} - \frac{B_\phi}{\mu_0 \rho R_0 \sin\theta}\frac{\partial b_\phi}{\partial \phi} - \frac{B_\phi}{\mu_0 \rho R_0}\frac{\cos\theta}{\sin\theta} b_\theta = 0, \tag{2b}$$

$$\frac{\partial h}{\partial t} + \frac{H_0}{R_0 \sin\theta}\frac{\partial}{\partial \theta}(\sin\theta u_\theta) + \frac{H_0}{R_0 \sin\theta}\frac{\partial u_\phi}{\partial \phi} = 0, \tag{2c}$$

$$\frac{\partial b_\theta}{\partial t} - \frac{B_\phi}{R_0 \sin\theta}\frac{\partial u_\theta}{\partial \phi} = 0, \tag{2d}$$

$$\frac{\partial b_\phi}{\partial t} + \frac{1}{R_0}\frac{\partial}{\partial \theta}(u_\theta B_\phi) = \frac{B_\phi}{R_0 \sin\theta}\left\{\frac{\partial}{\partial \theta}(u_\theta \sin\theta) + \frac{\partial u_\phi}{\partial \phi}\right\}. \tag{2e}$$

In the above set of equations a toroidal magnetic field $B_\phi = B_0 \sin\theta$ was proposed by Zaqarashvili *et al.* (2007), and we adopt this here. This field can be generated in a full sphere by a uniform current in the z-direction, parallel to the rotation axis. The MHD waves for this field were studied by Malkus (1967) in the case of a full unstratified sphere.

The energy of our small perturbations comprises kinetic, potential and magnetic energy, so

$$E = \int_0^{2\pi}\int_0^{\pi}\left[\frac{\rho}{2}\left(u_\theta^2 + u_\phi^2\right) + \frac{g\rho}{2H_0}h^2 + \frac{1}{2\mu_0}\left(b_\theta^2 + b_\phi^2\right)\right]\sin\theta \,\mathrm{d}\theta \,\mathrm{d}\phi, \tag{3}$$

and we can deduce from Equations (2a)–(2e) that

$$\frac{\partial E}{\partial t} = \int_0^{2\pi}\int_0^{\pi}\left[\frac{2B_0 \cos\theta}{\mu_0 R_0}(u_\phi b_\theta - u_\theta b_\phi)\right]\sin\theta \,\mathrm{d}\theta \,\mathrm{d}\phi. \tag{4}$$

In the nonmagnetic case, the disturbance energy is constant, and since it has a positive definite form, it is not possible for unstable growing modes to occur. However, in the magnetic case it is possible for the disturbance energy to grow, so unstable modes are possible in this system. As we shall see below, for some parameter values only wave-like disturbances are possible, but for other values instability can occur.

3. Method for determining the eigenvalues and eigenvectors

The solutions are in the form $\mathrm{e}^{\mathrm{i}m\phi - \mathrm{i}\omega t}$, where ϕ is the longitude, m is the azimuthal wave number and t is the time, which leads to a set of five coupled ordinary differential equations with θ as the independent variable. We express these in dimensionless form, using $2\Omega_0 R_0$

as the velocity scale and B_0 as the magnetic field scale, to obtain, defining $\mu = \cos\theta$ and the differential operator $\mathrm{D} = -\sin\theta\partial/\partial\theta = (1-\mu^2)\partial/\partial\mu$,

$$-\lambda\tilde{u}_\theta + \mu\tilde{u}_\phi + \mathrm{D}\eta - m\alpha^2\tilde{b}_\theta - 2\alpha^2\mu\tilde{b}_\phi = 0, \tag{5a}$$

$$\lambda\tilde{u}_\phi - \mu\tilde{u}_\theta - m\eta + m\alpha^2\tilde{b}_\phi + 2\alpha^2\mu\tilde{b}_\theta = 0, \tag{5b}$$

$$\lambda\epsilon(1-\mu^2)\eta + \mathrm{D}\tilde{u}_\theta - m\tilde{u}_\phi = 0, \tag{5c}$$

$$\lambda\tilde{b}_\theta + m\tilde{u}_\theta = 0, \tag{5d}$$

$$\lambda\tilde{b}_\phi + m\tilde{u}_\phi = 0. \tag{5e}$$

Here these scaled variables, which are now functions of θ only, are related to the dimensional variables by

$$u_\theta = \mathrm{Re}\left\{\frac{2\mathrm{i}\Omega_0 R_0\tilde{u}_\theta}{\sin\theta}\mathrm{e}^{\mathrm{i}(m\phi-\lambda t)}\right\}, \qquad b_\theta = \mathrm{Re}\left\{\frac{\mathrm{i}B_0\tilde{b}_\theta}{\sin\theta}\mathrm{e}^{\mathrm{i}(m\phi-\lambda t)}\right\}, \tag{6a,b}$$

$$u_\phi = \mathrm{Re}\left\{\frac{2\Omega_0 R_0\tilde{u}_\phi}{\sin\theta}\mathrm{e}^{\mathrm{i}(m\phi-\lambda t)}\right\}, \qquad b_\phi = \mathrm{Re}\left\{\frac{B_0\tilde{b}_\phi}{\sin\theta}\mathrm{e}^{\mathrm{i}(m\phi-\lambda t)}\right\}, \tag{6c,d}$$

$$h = \mathrm{Re}\left\{\frac{4\Omega_0^2R_0^2\eta}{g}\mathrm{e}^{\mathrm{i}(m\phi-\lambda t)}\right\}, \tag{6e}$$

and the dimensionless parameters and the dimensionless frequency are

$$\epsilon = \frac{4\Omega_0^2R_0^2}{gH_0}, \qquad \alpha^2 = \frac{v_A^2}{4\Omega_0^2R_0^2}, \qquad \text{where} \qquad v_A^2 = \frac{B_0^2}{\mu_0\rho}, \qquad \lambda = \frac{\omega}{2\Omega_0}. \tag{7a–d}$$

From (5d,e) we see that for axisymmetric $m = 0$ modes, the magnetic field perturbations are zero, so that there is no difference between the magnetic and non-magnetic case for $m = 0$ modes. Since the $m = 0$ modes are discussed in Longuet-Higgins (1968), we do not consider them further here.

The solutions for the dependent variables are taken as expansions of Associated Legendre Polynomials, following Longuet-Higgins (1968), remembering that each expansion must have $n \geq m$ because the polynomials are not defined for $n < m$,

$$\tilde{u}_\theta = \sum_{n=m}^{\infty} A_n^m \mathrm{P}_n^m(\mu), \qquad \tilde{b}_\theta = \sum_{n=m}^{\infty} B_n^m \mathrm{P}_n^m(\mu), \tag{8a,b}$$

$$\tilde{u}_\phi = \sum_{n=m}^{\infty} C_n^m \mathrm{P}_n^m(\mu), \qquad \tilde{b}_\phi = \sum_{n=m}^{\infty} D_n^m \mathrm{P}_n^m(\mu), \tag{8c,d}$$

$$\eta = \sum_{n=m}^{\infty} E_n^m \mathrm{P}_n^m(\mu). \tag{8e}$$

Some properties of associated Legendre polynomials are used:

$$\mu \mathrm{P}_n^m = \frac{(n+m)}{(2n+1)}\mathrm{P}_{n-1}^m + \frac{(n-m+1)}{(2n+1)}\mathrm{P}_{n+1}^m,$$
$$D\mathrm{P}_n^m = \frac{(n+1)(n+m)}{(2n+1)}\mathrm{P}_{n-1}^m - \frac{n(n-m+1)}{(2n+1)}\mathrm{P}_{n+1}^m.$$

Substituting the expansions of the dependent variables into Equations (5a–e) and then using the properties of the associated Legendre Polynomials, we obtain a set of equations. In each equation we must set the coefficient of $\mathrm{P}_n^m(\mu)$ to zero, and we then obtain the following equations for the coefficients in our expansion, A_n^m, B_n^m, C_n^m, D_n^m, E_n^m:

$$\begin{aligned}
-\lambda A_n^m &= m\alpha^2 B_n^m - q_{n-1}C_{n-1}^m + 2\alpha^2 q_{n-1}D_{n-1}^m + (n-1)q_{n-1}E_{n-1}^m \\
&\quad - p_{n+1}C_{n+1}^m + 2\alpha^2 p_{n+1}D_{n+1}^m - (n+2)p_{n+1}E_{n+1}^m, \qquad (9a)\\
\lambda C_n^m &= mE_n^m - m\alpha^2 D_n^m + q_{n-1}A_{n-1}^m \\
&\quad - 2\alpha^2 q_{n-1}B_{n-1}^m - 2\alpha^2 p_{n+1}B_{n+1}^m + p_{n+1}A_{n+1}^m, \qquad (9b)\\
\lambda\left[\epsilon(1-p_n q_{n-1} \right.& \left. -q_n p_{n+1})E_n^m - \epsilon p_{n+2}p_{n+1}E_{n+2}^m - \epsilon q_{n-1}q_{n-2}E_{n-2}^m\right] \\
&= mC_n^m - (n+2)p_{n+1}A_{n+1}^m + (n-1)q_{n-1}A_{n-1}^m, \qquad (9c)\\
\lambda B_n^m &= -mA_n^m, \qquad (9d)\\
\lambda D_n^m &= -mC_n^m, \qquad (9e)
\end{aligned}$$

where $q_n = (n-m+1)/(2n+1)$ and $p_n = (n+m)/(2n+1)$.

3.1. Parity of the modes

Equations (9a–e) have a special parity. For a given m, the coefficients A_n^m and B_n^m with n even are related only to the C_n^m, D_n^m and E_n^m coefficients with n odd. Similarly, the coefficients A_n^m and B_n^m with n odd are related only to the C_n^m, D_n^m and E_n^m coefficients with n even. The equations therefore form two distinct sets. We solve each set separately using a MATLAB eigenvalue and eigenvector solver, designed to solve the system of equations $\mathsf{A}\boldsymbol{v} = \lambda\mathsf{B}\boldsymbol{v}$.

The associated Legendre polynomials are symmetric about the equator if $n-m$ is even, and antisymmetric if $n-m$ is odd. Of the two sets of modes with different parities, we call the set with $\tilde{u}_\theta$ and $\tilde{b}_\theta$ symmetric about the equator the sinuous modes, since fluid will flow northwards at the equator in some locations and southward in others. For a sinuous (or kink) mode η, $\tilde{u}_\phi$ and $\tilde{b}_\phi$ are antisymmetric about the equator, and the expansions for $\tilde{u}_\theta$ and $\tilde{b}_\theta$ in (17) start with A_m^m, and B_m^m, while the expansions for $\tilde{u}_\phi$, $\tilde{b}_\phi$ and η start with C_{m+1}^m, D_{m+1}^m and E_{m+1}^m respectively. The other set of modes are the varicose (or sausage) modes. These have $\tilde{u}_\theta$ and $\tilde{b}_\theta$ antisymmetric about the equator, so no flow or field crosses the equator for varicose modes. The varicose modes have η, $\tilde{u}_\phi$ and $\tilde{b}_\phi$ symmetric about the equator, and the expansions for $\tilde{u}_\theta$ and $\tilde{b}_\theta$ in (17) start with A_{m+1}^m and B_{m+1}^m, while the expansions for $\tilde{u}_\phi$, $\tilde{b}_\phi$ and η start with C_m^m, D_m^m and E_m^m.

3.2. Normalisation and numerical method

In our dimensionless units the energy (3) takes the form

$$E = 2\pi\rho\Omega_0^2 R_0^4 \int_0^\pi \left[\frac{|\tilde{u}_\theta|^2 + |\tilde{u}_\phi|^2}{\sin^2\theta} + \alpha^2 \frac{|\tilde{b}_\phi|^2 + |\tilde{b}_\theta|^2}{\sin^2\theta} + \epsilon|\eta|^2 \right] \sin\theta \, \mathrm{d}\theta. \tag{10}$$

For a purely wave-like disturbance this energy is constant in time. Following Longuet-Higgins (1968), we set the energy

$$E \equiv 2\pi\rho H_o \Omega_0^2 R_0^4.$$

Substituting this into (10) we obtain

$$\int_0^\pi \left[\frac{|\tilde{u}_\theta|^2 + |\tilde{u}_\phi|^2}{\sin^2\theta} + \alpha^2 \frac{|\tilde{b}_\phi|^2 + |\tilde{b}_\theta|^2}{\sin^2\theta} + \epsilon|\eta|^2 \right] \sin\theta \, \mathrm{d}\theta = 1, \tag{11}$$

which defines the way in which our eigenfunctions are normalised.

In the case when there are unstable waves, the energy is not constant, but nevertheless (11) continues to provide a convenient normalisation. We let $\lambda = \lambda_r + \mathrm{i}\sigma$, where σ is the dimensionless growth rate, and in terms of the dimensionless variables we can write (4) as

$$\begin{aligned} \sigma \int_0^\pi \left[\frac{|\tilde{u}_\theta|^2 + |\tilde{u}_\phi|^2}{\sin^2\theta} + \alpha^2 \frac{|\tilde{b}_\phi|^2 + |\tilde{b}_\theta|^2}{\sin^2\theta} + \epsilon|\eta|^2 \right] \sin\theta \mathrm{d}\theta \\ = \alpha^2 \int_0^\pi \mathrm{i}(\tilde{u}_\theta^* \tilde{b}_\phi + \tilde{u}_\phi^* \tilde{b}_\theta - \tilde{u}_\theta \tilde{b}_\phi^* - \tilde{u}_\phi b_\theta^*) \frac{\cos\theta}{\sin\theta} \, \mathrm{d}\theta. \end{aligned} \tag{12}$$

For neutrally stable waves, the scaled (tilde) variables are pure real, so the right hand side is zero, consistent with $\sigma = 0$. We can use (5d) and (5e) to simplify (12) to obtain

$$\sigma \int_0^\pi \left[\frac{|\tilde{u}_\theta|^2 + |\tilde{u}_\phi|^2}{\sin^2\theta} + \alpha^2 \frac{(|\tilde{b}_\phi|^2 + |\tilde{b}_\theta|^2)}{\sin^2\theta} + \epsilon|\eta|^2 + \frac{\alpha^2 \cos\theta}{m \sin^2\theta} (\tilde{b}_\theta^* \tilde{b}_\phi + \tilde{b}_\phi^* \tilde{b}_\theta) \right] \sin\theta \, \mathrm{d}\theta = 0. \tag{13}$$

It is clear that for growing modes, the last magnetic term in the integral in this equation must be negative, to balance the other positive definite terms coming from the disturbance energy.

The numerical procedure to solve the eigenvalue problem is to truncate the expansions in (17) and to then derive a matrix eigenvalue equation which is solved using MATLAB. We illustrate using the sinuous mode case, the program for the varicose mode case being similar. We set

$$\tilde{u}_\theta = \sum_{n=0}^{N-1} A_{m+2n}^m \mathrm{P}_{m+2n}^m(\mu) \, \mathrm{e}^{\mathrm{i}m\phi - \mathrm{i}\omega t}, \qquad \tilde{b}_\theta = \sum_{n=0}^{N-1} B_{m+2n}^m \mathrm{P}_{m+2n}^m(\mu) \, \mathrm{e}^{\mathrm{i}m\phi - \mathrm{i}\omega t}, \tag{14a,b}$$

$$\tilde{u}_\phi = \sum_{n=1}^{N} C_{m+2n-1}^m \mathrm{P}_{m+2n-1}^m(\mu) \, \mathrm{e}^{\mathrm{i}m\phi - \mathrm{i}\omega t}, \quad \tilde{b}_\phi = \sum_{n=1}^{N} D_{m+2n-1}^m \mathrm{P}_{m+2n-1}^m(\mu) \, \mathrm{e}^{\mathrm{i}m\phi - \mathrm{i}\omega t}, \tag{14c,d}$$

$$\eta = \sum_{n=1}^{N} E_{m+2n-1} n^m \mathrm{P}^m_{m+2n-1}(\mu)\, \mathrm{e}^{\mathrm{i}m\phi - \mathrm{i}\omega t}. \tag{14e}$$

We then use Equations (5a–e) to derive a $5N \times 5N$ algebraic eigenvalue problem to obtain $5N$ approximate eigenvalues λ. The eigenvectors emerging from our MATLAB must be normalised to satisfy (11), so we use the unnormalised eigenvectors to evaluate

$$\begin{aligned} E' = \sum_{n=1}^{N}\sum_{k=1}^{N}\Big[&\big(A^m_{m+2n-2}\overline{A}^m_{m+2k-2} + \alpha^2 B^m_{m+2n-2}\overline{B}^m_{m+2kn-2}\big) I^m_{m+2n-2,m+2k-2} \\ &+ \big(C^m_{m+2n-1}\overline{C}^m_{m+2k-1} + \alpha^2 D^m_{m+2n-1}\overline{D}^m_{m+2n-1}\big) I^m_{m+2n-1,m+2k-1}\Big] \\ &+ \sum_{n=1}^{N} \epsilon E^m_{m+2n-1}\overline{E}^m_{m+2n-1}\frac{2(2m+2n-1)\,!}{(2m+4n-11)(2n-1)\,!}, \end{aligned} \tag{15}$$

where $\bar{}$ denotes complex conjugate. The integral in the last equation has an exact formula given by

$$I^m_{nk} = \int_{-1}^{1} \frac{\mathrm{P}^m_n(x)\mathrm{P}^m_k(x)}{(1-x^2)}\,\mathrm{d}x = \frac{(n+m)\,!}{m(n-m)\,!},$$

for $n < k$ when n and k have the same parity,

$$I^m_{nk} = \int_{-1}^{1} \frac{\mathrm{P}^m_n(x)\mathrm{P}^m_k(x)}{(1-x^2)}\,\mathrm{d}x = \frac{(k+m)\,!}{m(k-m)\,!},$$

for $k < n$ when n and k have the same parity, and $I^m_{nk} = 0$ when n and k have different parity. We then divide the eigenvectors by $\sqrt{E'}$ to obtain normalised eigenvectors that satisfy (11). We then use (14a,b) to construct the eigenfunctions corresponding to each eigenvalue. Only the eigenvalues corresponding to eigenvectors which drop off rapidly as n increases are reliable converged solutions. We therefore constructed a criterion based on the relative magnitude of the sum of the squares of components above and below $n = N/2$. Only solutions with the great majority of the power in the lower half of the spectrum were accepted. For these acceptable solutions increasing N did not change the eigenvalue significantly.

For the sinuous modes, the values of n for the coefficients A^m_n and B^m_n are $n = m, m+2, m+4, \ldots$, and for C^m_n, D^m_n and E^m_n they are $n = m+1, m+3, m+5, \ldots$. For the varicose modes, the index runs in the opposite way, following the parity rules in Section 3.1.

3.3. Second order ODE formulation

When using asymptotic methods, it is convenient to start with the system in the form of a single second order equation. Two equations proved useful, one for the variable $\tilde{u}_\theta$, the other for the variable η. Although these are both complicated, they are useful because they

can be simplified in a number of limits to give well-known equations. The equation for $\tilde{u}_\theta$ can be written

$$(1-\mu^2)\frac{\mathrm{d}^2\tilde{u}_\theta}{\mathrm{d}\mu^2}+\frac{2m^2}{(\lambda^2-\alpha^2m^2)\epsilon(1-\mu^2)-m^2}\mu\frac{\mathrm{d}\tilde{u}_\theta}{\mathrm{d}\mu} +\left[\epsilon(\lambda^2-\alpha^2m^2)-\frac{m(\lambda+2m\alpha^2)}{(\lambda^2-\alpha^2m^2)}-\epsilon\frac{(\lambda+2m\alpha^2)^2}{(\lambda^2-\alpha^2m^2)}\mu^2 -\frac{m^2}{1-\mu^2}-\frac{2\epsilon m(\lambda+2m\alpha^2)\mu^2}{(\lambda^2-\alpha^2m^2)\epsilon(1-\mu^2)-m^2}\right]\tilde{u}_\theta=0, \tag{16}$$

and equation for η is

$$(1-\mu^2)\frac{\mathrm{d}^2\eta}{\mathrm{d}\mu^2}+2\left(\frac{(\lambda+2m\alpha^2)^2(1-\mu^2)}{(\lambda^2-m^2\alpha^2)^2-(\lambda+2m\alpha^2)^2\mu^2}-1\right)\mu\frac{\mathrm{d}\eta}{\mathrm{d}\mu} +\left[\frac{-m(\lambda+2m\alpha^2)}{(\lambda^2-m^2\alpha^2)}-\frac{m^2}{1-\mu^2}+\epsilon\left((\lambda^2-m^2\alpha^2)-\frac{(\lambda+2m\alpha^2)^2\mu^2}{\lambda^2-m^2\alpha^2}\right) +\frac{2m(\lambda+2m\alpha^2)(\lambda^2-m^2\alpha^2)}{(\lambda^2-m^2\alpha^2)^2-(\lambda+2m\alpha^2)^2\mu^2}\right]\eta=0. \tag{17}$$

We note here that, if one defines

$$L=\frac{(\lambda^2-m^2\alpha^2)}{(\lambda+2m\alpha^2)}, \qquad E=\epsilon\frac{(\lambda^2-m^2\alpha^2)}{L^2},$$

then (17) reduces to

$$(1-\mu^2)\frac{\mathrm{d}^2\eta}{\mathrm{d}\mu^2}+2\frac{(1-L^2)}{(L^2-\mu^2)}\mu\frac{\mathrm{d}\eta}{\mathrm{d}\mu}+\left[\frac{-m}{L}-\frac{m^2}{1-\mu^2}+E(L^2-\mu^2)+\frac{2mL}{L^2-\mu^2}\right]\eta=0. \tag{18}$$

This is an apparent simplification from four to three independent parameters. However L and E can not be considered as input parameters as they both depend on the eigenvalue λ.

4. Hydrodynamic case

In the absence of magnetic field, the set of five equations reduces to three equations, the Laplace tidal equations which have been extensively studied by Longuet-Higgins (1968). He found two different kind of waves when ϵ is small: gravity waves and Rossby waves. Gravity waves are produced by the action of gravity on the interface giving the restoring force in the system. They are common in stably stratified layers of fluid and can propagate either vertically or horizontally, Gill (1982). Note that though our model has a sharp interface at the boundary of the stable layer, the horizontal propagation of gravity waves in a continuously stratified system behaves similarly. In the limit $\epsilon \to 0$ their dispersion relation has the form

$$\omega=\pm\frac{\sqrt{n(n+1)gH_0}}{R_0}, \qquad \text{and so} \qquad \lambda=\pm\sqrt{\frac{n(n+1)}{\epsilon}} \tag{19a,b}$$

and the eigenfunctions become surface spherical harmonics (Longuet-Higgins 1968), i.e. the coupling between adjacent harmonics becomes negligible. The parameter n is the degree of the spherical harmonic, and so gives the number of nodes in the latitudinal direction. As ϵ increases, rotation becomes important and the gravity modes turn into inertia-gravity waves, and the eigenfunctions are no longer simple spherical harmonics, but the parameter n is still useful in classifying the eigenfunctions, and we continue to use it as did Longuet-Higgins (1968).

The Rossby waves are produced by the effect of the rotation of the fluid system. In the Earth, they arise from the latitudinal variation of the Coriolis force, $2\boldsymbol{\Omega} \times \boldsymbol{u}$. The dispersion relation of these waves is

$$\omega = -\frac{2\Omega_0 m}{n(n+1)} \qquad \text{and} \qquad \lambda = -\frac{m}{n(n+1)}. \tag{20a,b}$$

From the minus sign it is clear that these waves travel to the west. Their frequency is independent of ϵ.

When ϵ is large, the solution is confined to the neighbourhood of the equator where the limit $\mu^2 \ll 1$ is valid, Longuet-Higgins (1968). Then, there are three dispersion relations for the approximated solutions. The dispersion relation for gravity waves is

$$\lambda = \pm\frac{(2\nu+1)^{1/2}}{\epsilon^{1/4}} + \frac{m}{\epsilon^{1/2}(4\nu+2)} \qquad \text{for integer} \quad \nu \geq 0. \tag{21}$$

The parameter ν is the eigenvalue of the parabolic cylinder function, see Longuet-Higgins (1968) and Section 6.1.1. ν gives the number of nodes in the latitudinal direction in the trapped case.

The dispersion relation of Rossby waves at large ϵ has the formula

$$\lambda = -\frac{m}{\epsilon^{1/2}(2\nu+1)} \qquad \text{for integer} \quad \nu \geq 1. \tag{22}$$

As noted by Longuet-Higgins (1968) the $\nu = 0$ case does not lead to a valid asymptotic solution. Finally, the Kelvin waves have the dispersion relation given by

$$\lambda \sim \frac{m}{\epsilon^{1/2}}. \tag{23}$$

Kelvin waves have the property that the northward velocity $\hat{u}_\theta$ tends to zero rapidly as ϵ increases, and the waves are equatorially trapped.

An interesting question is how the different n modes in the small ϵ theory connect to the different ν modes in the large ϵ theory as ϵ is gradually increased. For eastward propagating gravity modes, the frequencies evolve continuously from the n value in (19a,b) with the + sign to the

$$\nu = n - m - 1 \qquad \text{eastward propagating gravity waves} \tag{24}$$

solution with the plus sign in (21). An exceptional case is the $n = m$ mode in (19a,b), which evolves into the Kelvin mode at large ϵ. The westward gravity waves given by (19a,b) evolve into the equatorially trapped gravity waves given by (21) with

$$\nu = n - m + 1 \qquad \text{westward propagating gravity waves} \tag{25}$$

for all $n \geq m$. The westward Rossby waves given by (20a,b) at small ϵ evolve into large ϵ equatorially trapped Rossby wave solutions given by (22) with $\nu = n - m$. However, since $\nu = 0$ is not available in (22), the $n = m$ Rossby mode at small ϵ evolves continuously into the $\nu = 0$ gravity mode given by (21). This exceptional mode is known as a mixed Rossby-gravity wave. In this way, there is one-to-one matching between the solutions at small ϵ given by (19a,b) and (20a,b) and the large ϵ solutions given by (21)–(23).

Generally, there was good agreement between our numerical results and those of Longuet-Higgins (1968), except for some slight differences in the trapped cases, where a resolution higher than that available to Longuet-Higgins (1968) was required to get full accuracy. Generally the solutions converge when the expansions are truncated at $N = 40$.

5. Magnetohydrodynamic case: numerical solutions

We now consider the effect of the magnetic field using our eigenvalue code. The parameters we can vary are ϵ, the azimuthal wavenumber m, and the parameter α which measures the magnetic field strength. A truncation parameter $N = 70$ was found to be adequate to resolve all the modes displayed in our figures. The effect of the magnetic field is to split the hydrodynamic Rossby waves into two modes: slow and fast magnetic Rossby modes. The Kelvin waves and the gravity are also affected by the magnetic field. We call the branch that develops from the gravity waves MIG waves, as they are inertio-gravity waves, in which Coriolis and gravity forces are important, combined with the magnetic Lorentz force.

Numerical dispersion diagrams computed for $\alpha = 0.1$ and $m = 1$ are shown in Figure 1, with $\lambda = \omega/2\Omega_0$ plotted against $\epsilon^{-1/2} = \sqrt{gH_0}/2\Omega_0 R_0$. Figure 1(a) shows the eastward propagating waves: the MIG waves in dotted-red, the Kelvin mode in dashed-green and the slow magnetic Rossby waves in solid blue. The MIG waves form an infinite sequence with increasing frequency and a corresponding increase in the number of nodes in the latitudinal direction. Only the lowest two MIG modes are shown in Figure 1(a).

The MIG eigenfunction sequence is shown in Figure 2(a) where $\tilde{u}_\theta / \sin\theta$ is plotted as a function of co-latitude. The lowest frequency mode (solid blue) is a sinuous mode, the next is a varicose mode (dashed green), and the next sinuous mode (dotted red) is also shown. From Figure 1(a) we see that as $\epsilon \to 0$ the MIG wave frequencies scale linearly with $\epsilon^{-1/2}$ showing that their frequency in this low rotation limit scales with $\sqrt{gH_0}/R_0$ indicating their gravity wave character. The Kelvin mode is exceptional, only a single varicose mode, and it too scales with $\sqrt{gH_0}/R_0$ at small rotation, as do non-magnetic Kelvin waves. The eigenfunction for the Kelvin mode is shown in Figure 2(b). The eastward propagating slow magnetic Rossby waves are shown in solid blue in Figure 1(a). These waves have no counterpart in the non-magnetic case, and their frequency tends to zero as $\alpha \to 0$. In the slow rotation limit $\epsilon \to 0$ the slow magnetic Rossby wave dispersion curve levels out, showing that the frequency scales with rotation rate for these waves. The eigenfunctions for the slow magnetic Rossby waves are shown in Figure 3(b). The sequence alternates between sinuous modes and varicose (or sausage) modes with the slowest mode being a varicose mode, the next slowest a sinuous mode, and then comes a second varicose mode. As is shown in Figure 2(a), the blue solid curve has two nodes in latitude, the green dashed line three nodes and the dotted red one four nodes. There is, of course, a complete sequence of increasing number of nodes as well as increasing frequencies.

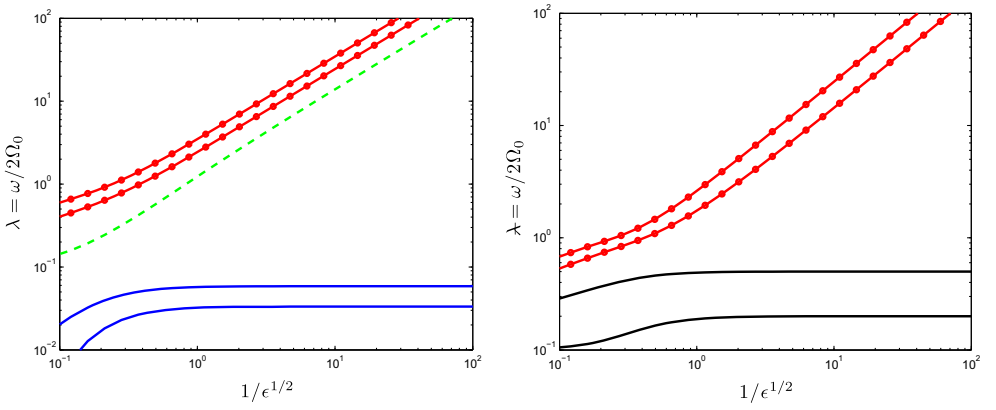

(a) Eastward (b) Westward

Figure 1. Dispersion relation $\lambda = \omega/2\Omega_0$ as a function of $1/\epsilon^{1/2} = \sqrt{gH_0}/2\Omega_0 R_0$, for $\alpha = 0.1$ and $m = 1$. (a) Waves travelling eastward: the red dotted curves are Magneto-Inertial-Gravity waves, the green dashed line is the Kelvin mode, whereas the blue solid lines correspond to slow magnetic Rossby modes. (b) Waves travelling westwards: the red dotted curves are two Magneto-Inertial-Gravity modes. The higher solid black curve is the mixed Rossby-gravity wave, and the lower black solid curve is a fast magnetic Rossby wave.

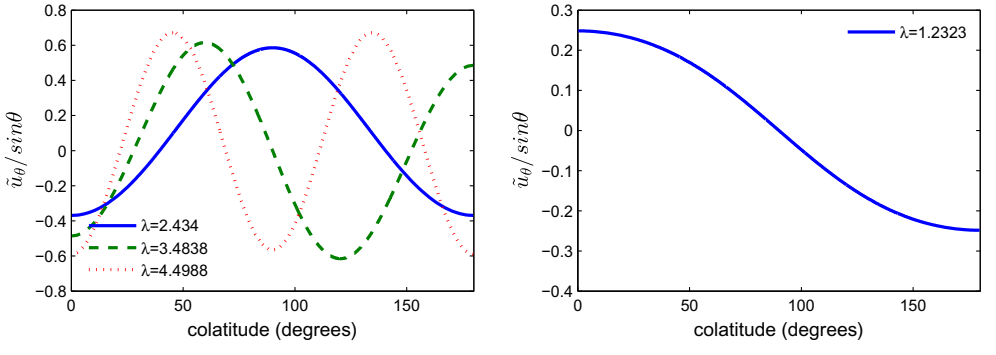

(a) MIG waves (b) Kelvin wave

Figure 2. Eigenfunctions $\tilde{u}_\theta / \sin\theta$ against co-latitude, for $m = 1$, $N = 50$, $\alpha = 0.1$ and $\epsilon = 1$. (a) MIG waves travelling eastwards, the fastest and slowest being sinuous modes, the intermediate frequency wave being a varicose mode. When the frequency increases the number of nodes increases too. (b) Kelvin mode which is a varicose mode.

In Figure 1(b) we show some westward propagating waves. The MIG waves behave similarly to the eastward propagating MIG waves, and as $\epsilon \to 0$ the frequencies occur in pairs, one eastward, one westward as expected since rotation plays no role for MIG waves in this limit. The two black solid curves are fast magnetic Rossby waves. In the limit as $\alpha \to 0$ these merge into the hydrodynamic Rossby waves found by Longuet-Higgins (1968).

Figure 3(a) shows the first three fast magnetic Rossby modes, a sinuous mode without nodes is the blue solid curve, the fastest of these waves, the green dashed line is a varicose mode with one node and the red dotted curve is a second sinuous mode with two nodes.

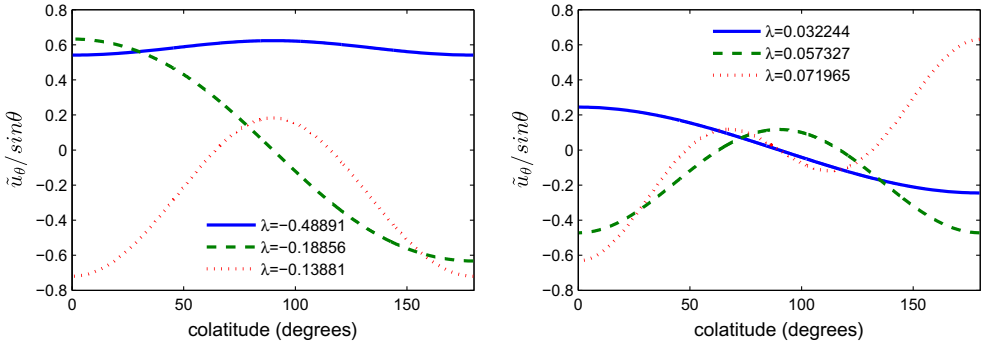

(a) Fast Magnetic Rossby waves (b) Slow Magnetic Rossby waves

Figure 3. Eigenfunctions $\tilde{u}_\theta / \sin\theta$ against co-latitude ($m = 1$, $N = 50$, $\alpha = 0.1$ and $\epsilon = 1$). (a) Fast Magnetic Rossby waves travelling westwards, the blue solid curve represents the fastest sinuous mode, the green dashed curve being the fastest varicose mode. The red dotted curve is a slower sinuous mode. The number of nodes increases when the frequency decreases in magnitude. (b) Slow Magnetic Rossby waves travelling eastwards. Note that solid blue and dotted red modes are varicose modes with one and three nodes respectively,the green dashed curve is a sinuous mode with two nodes. Slow Rossby waves increase in frequency as the number of nodes increases.

Slow magnetic Rossby waves plotted in 3(b) have the following sequence: the slowest first mode shown in solid blue is a varicose mode with one node, the next in dashed green is a sinuous mode with two nodes and the third (dotted red) varicose mode has three nodes.

5.1. MIG waves

Solving the eigenvalue problem with a MATLAB code, we found numerically that the highest frequencies correspond to MIG waves. These waves are essentially (Longuet-Higgins 1968) class 1 waves, interfacial gravity waves, modified by the magnetic field. Using (17) for η, we let $\epsilon \to 0$, with $\lambda \sim \mathrm{O}(\epsilon^{-1/2})$, the gravity wave scaling. Then provided α is not too large, $\alpha = \mathrm{O}(\epsilon^{-1/2})$, the η-Equation (17) reduces to the associated Legendre equation, with solutions $\eta = \mathrm{P}_n^m(\cos\theta)$ and λ is governed by (19a,b). So in the $\epsilon \to 0$ limit, provided the magnetic field is not too strong, the solutions for η are spherical harmonics.

In Figure 4, the top two panels show η for the P_2^1 MIG wave with $\epsilon = 1$. The P_2^1 mode is not the slowest $m = 1$ mode, that is the P_1^1 varicose mode gravity wave, but it is the lowest frequency sinuous mode and is representative of the behaviour of the general case. At small ϵ, even for α as large as 5 the solutions are very similar to Figure 4(a). However, the two top panels of Figure 4 at $\epsilon = 1$ show a marked difference between the $\alpha = 10^{-3}$ and $\alpha = 5$ cases. The small magnetic field solution is still essentially a P_2^1 spherical harmonic, but the stronger magnetic field has caused the mode to concentrate near the equator, so it is becoming an equatorially trapped mode. At $\epsilon = 100$, the bottom two panels, we see in Figure 4(c) that even when the magnetic field is too weak to affect the solution the wave becomes equatorially trapped. The $\alpha = 5$, $\epsilon = 100$ case is completely trapped at the equator, and required a truncation level of $N = 70$ to resolve it. It is clear from these results that as either $\epsilon \to \infty$ or as $\alpha \to \infty$ MIG waves become equatorially trapped. In Section 6 we develop an asymptotic theory which sheds light on the behaviour in both these

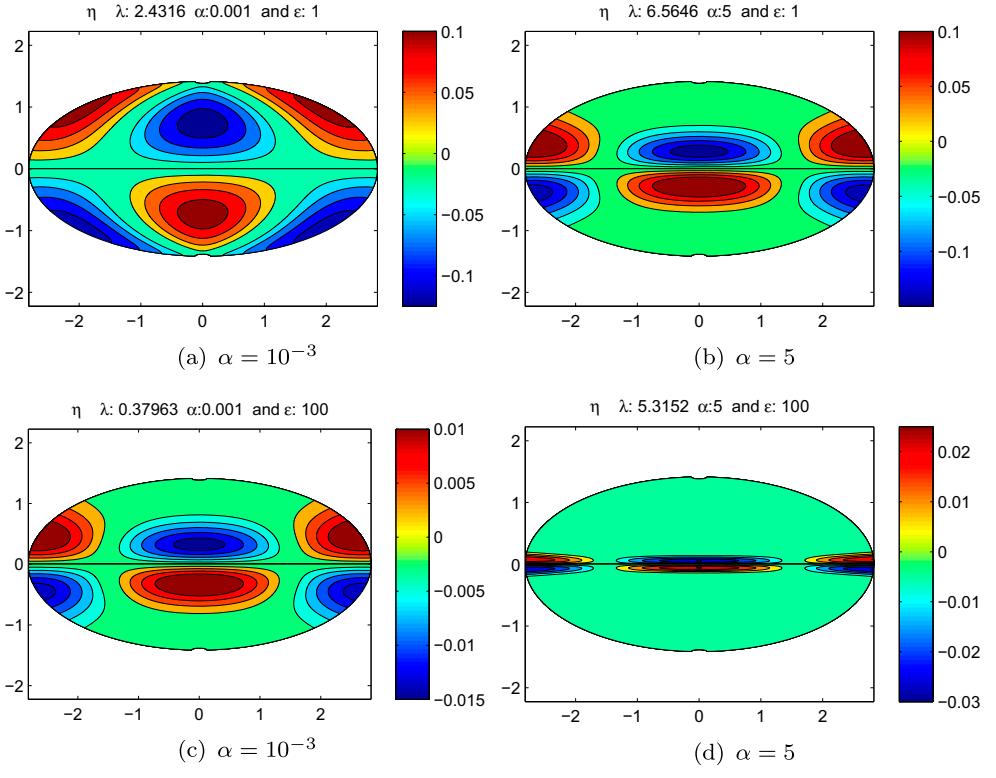

Figure 4. Contour plots of the scaled height η with ϵ 1 and 100. These are numerical solutions for MIG waves travelling eastward, and the sequence corresponds to the P_2^1 spherical harmonic at small ϵ and α. The left column corresponds to $\alpha = 10^{-3}$ with $N = 50$ and the right column to $\alpha = 5$ with $N = 70$.The bottom right panel shows strong equatorial trapping.

limits. An interesting feature of these solutions is that the amplitude of the η disturbance becomes small compared to unity as ϵ increases. This means that most of the energy of the disturbance is kinetic and magnetic energy at large ϵ with very little in the form of potential energy.

In Table 1 (eastward propagating waves) and 2 (westward propagating waves) we set $m = 1$ and looked for the solution that corresponds to the P_2^1 solution in the low ϵ, low α limit. As ϵ or α are increased, this mode evolves continuously, giving the results shown in the two tables. At large ϵ and small α we know that the table 1 results must agree asymptotically with the $\nu = 0$ (21) formula, recalling from Section 4 that eastward gravity waves have the connection formula $\nu = n - m - 1$, and the table 2 results must agree with the $\nu = 2$ (21) formula, as westward gravity waves connect ν with $n - m + 1$. Since only the rotation distinguishes between the magnitude of the frequencies of eastward and westward propagating waves, the differences (apart from the sign) are only significant at large values of ϵ. Even then, when α becomes large the waves take the form of Alfvén waves which have the same form whether travelling eastward or westward. As α is increased, the MIG waves in both directions merge smoothly into Alfvén waves. These Alfvén wave modes become increasingly trapped at the equator as α increases. The entries for large α and large ϵ are not shown, because these modes are so equatorially trapped they need a very high

Table 1. Eigenvalues λ for different values of α and ϵ, $N = 50$ and $m = 1$. Numerical solutions for MIG waves: waves travelling eastward. These are the $n = 2$ solutions with eigenfunctions as in Figure 4. The starred entry at $\epsilon = 0.1, \alpha = 10^3$ required $N = 80$.

α	10^{-3}	10^{-2}	10^{-1}	1	10^{1}	10^{2}	10^{3}
$\epsilon = 0.01$	24.419	24.419	24.419	24.434	26.269	117.86	1037.1
$\epsilon = 0.1$	7.6851	7.6851	7.6856	7.7409	14.357	108.09	1017.2*
$\epsilon = 1$	2.4316	2.4316	2.434	2.6913	11.839	103.72	****
$\epsilon = 10$	0.8459	0.84601	0.85661	1.5451	10.833	****	****
$\epsilon = 100$	0.37963	0.37989	0.40424	1.2342	10.383	****	****

Table 2. Eigenvalues λ for different values of α and ϵ, $N = 50$ and $m = 1$. Numerical solutions for MIG waves: waves travelling westward. These are the $n = 2$ solutions with eigenfunctions as in Figure 4. The starred entry at $\epsilon = 0.1, \alpha = 10^3$ required $N = 80$.

α	10^{-3}	10^{-2}	10^{-1}	1	10^{1}	10^{2}	10^{3}
$\epsilon = 0.01$	−24.586	−24.586	−24.586	−24.598	−26.227	−117.74	−1037.1
$\epsilon = 0.1$	−7.8533	−7.8533	−7.8536	−7.8858	−14.102	−108.03	−1017.2*
$\epsilon = 1$	−2.6129	−2.6129	−2.6131	−2.6718	−11.719	−103.7	****
$\epsilon = 10$	−1.1119	−1.1118	−1.1088	−1.2956	−10.779	****	****
$\epsilon = 100$	−0.67845	−0.67845	−0.67891	−1.1118	−10.358	****	****

truncation N to resolve them. Fortunately, in this limit we have an asymptotic theory (see Section 6) which gives these missing frequencies to a high level of accuracy.

In Figure 5 we plot the corresponding eigenfunctions for $\tilde{u}_\theta / \sin\theta$ and $\tilde{u}_\phi / \sin\theta$ for the eastward and westward propagating modes. The modes shown here are sinuous modes continued from the solution which at small ϵ and α had η of the form P_2^1, as in Figure 4. The values shown are at a particular azimuthal angle ϕ, chosen so that the value at the equator of $u_\theta / \sin\theta$ is maximal. The behaviour at other longitudes may be inferred from the simple $\exp \mathrm{i}m\phi$ dependence. Recall that the unscaled variable u_θ is 90° out of phase with $\tilde{u}_\theta$. These plots also show clearly the equatorial trapping that occurs both for eastward and westward propagating waves. This equatorial trapping is reminiscent of that found by Zaqarashvili *et al.* (2009) who considered an antisymmetric basic state field with zero toroidal field at the equator. In that case the trapping was associated primarily with the variation of the magnetic field across the equator rather than the asymptotic nature of the parameters. The corresponding plots for the westward propagating MIG waves at large α (not shown) are almost identical to the eastward modes, because the rotation is only playing a very minor role. At large α it is the magnetic field that is trapping the wave at the equator.

5.2. Magnetic Rossby waves and instability

The small ϵ limit for magnetic Rossby waves is best derived from (16) rather than (17), Zaqarashvili *et al.* (2007). Unlike in the MIG wave case, we now take the limit $\epsilon \to 0$ with λ and α constant. Then Equation (16) reduces to

$$(1-\mu^2)\frac{\mathrm{d}^2\tilde{u}_\theta}{\mathrm{d}\mu^2} - 2\mu\frac{\mathrm{d}\tilde{u}_\theta}{\mathrm{d}\mu} + \left[-\frac{(\lambda+2m\alpha^2)m}{(\lambda^2-m^2\alpha^2)} - \frac{m^2}{(1-\mu^2)}\right]\tilde{u}_\theta = 0. \tag{26}$$

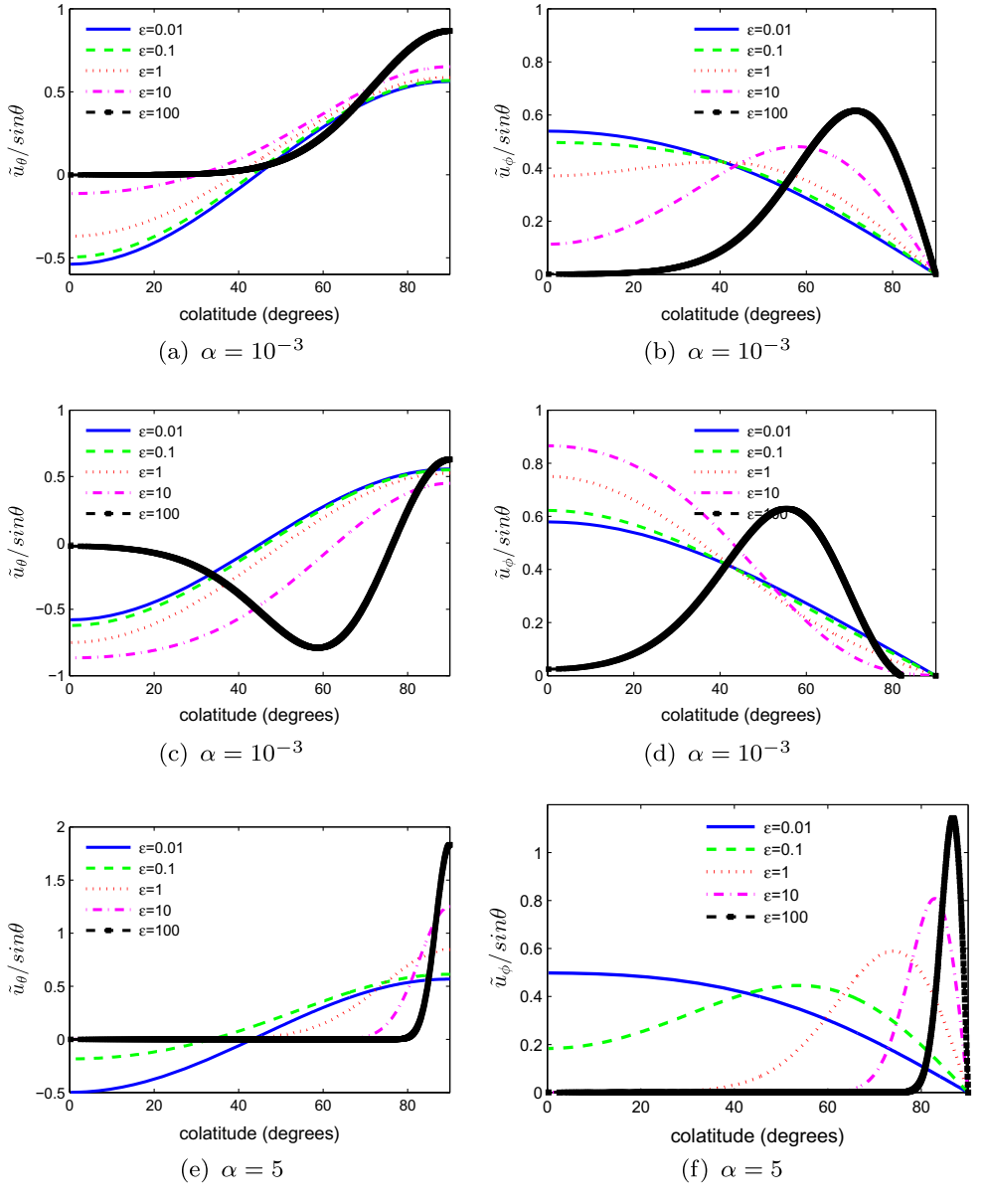

Figure 5. Northward and azimuthal velocities against co-latitude for different values of ϵ and α. These are MIG Waves with $N = 50$, $m = 1$ and $n = 2$, the slowest sinuous mode. (a) is $\tilde{u}_\theta / \sin\theta$ and (b) is $\tilde{u}_\phi / \sin\theta$ for the eastward propagating waves. (c) and (d) are similar for the westward propagating waves. (e) and (f) are for eastward propagating waves at much larger $\alpha = 5$, showing equatorial trapping. The westward propagating MIG waves at this value of α look almost identical.

This is again the Legendre differential equation, whose solutions are the associated Legendre polynomials, $\tilde{u}_\theta = \mathrm{P}_n^m(\cos\theta)$. The dispersion relation of these waves is

$$n(n+1) = -\frac{(\lambda + 2m\alpha^2)m}{(\lambda^2 - m^2\alpha^2)}, \tag{27}$$

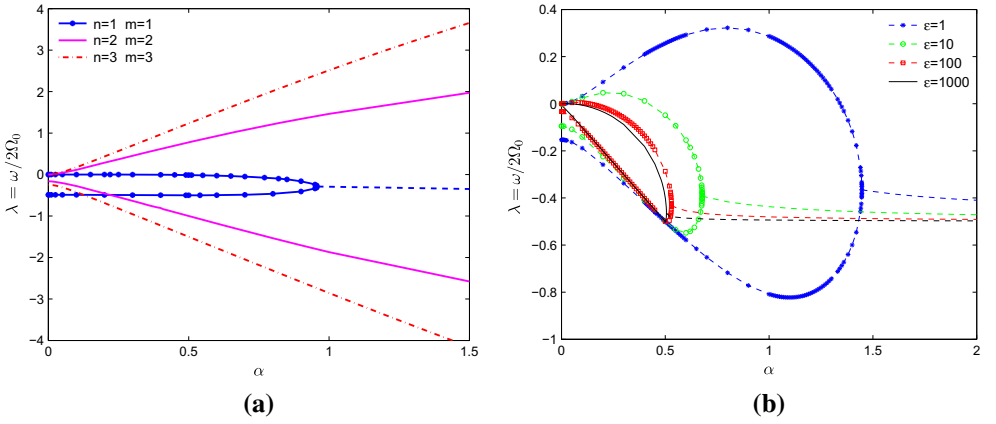

Figure 6. (a) Frequency of the magnetic Rossby waves at $\epsilon = 1$ as a function of α. The lowest modes are shown for $m = 1, 2, 3$. The upper branches are the slow magnetic Rossby waves, and the lower branch the fast magnetic Rossby waves. The two $m = 1$ branches merge near $\alpha = 0.956$ and a pair of complex modes branch off there. The dashed curve is the real part of the frequency of these complex modes. (b) The $m = 1$, $n = 2$ modes are shown for a range of different ϵ. The real parts of the frequency of the complex modes are shown as dashed lines.

where n is the latitudinal wave number and the degree of the Legendre polynomial. We have the following quadratic formula in λ,

$$n(n+1)\lambda^2 + m\lambda + m^2\alpha^2[2 - n(n+1)] = 0. \tag{28}$$

The solutions are

$$\lambda = \frac{-m \pm m\sqrt{1 - 4\alpha^2 n(n+1)[2 - n(n+1)]}}{2n(n+1)} \tag{29}$$

where the positive sign corresponds to slow magnetic Rossby waves, which travel eastward, and the negative sign gives the fast magnetic Rossby waves travelling westward. When $\alpha = 0$, equation for the fast Rossby modes reduces to $\lambda = -m/n(n+1)$ which are the hydrodynamic Rossby waves, Longuet-Higgins (1968). Note that $n = 1$ gives a zero frequency for the slow magnetic Rossby mode, but we see in Section 6.2.3 that at finite ϵ there is a very slow **westward** Rossby mode corresponding to $m = n = 1$, which we call the anomalous slow magnetic Rossby wave, as it travels in the opposite direction to all the other slow magnetic Rossby waves. So for each m there is a family of both slow and fast magnetic Rossby waves with n increasing from m to ∞. In Figure 6(a) we show how the frequencies of the magnetic Rossby waves evolve as α increases. Interestingly the $m = 1$ fast and slow magnetic Rossby branches merge together and a complex unstable branch emerges at this point. This means there are unstable growing modes in this model. Figure 6(a) is for the lowest frequency sinuous mode, but instability occurs for a whole family of $m = 1$ modes with increasingly complex θ structure. In Figure 6(b), which is for $m = 1$ but has $n = 2$, the first varicose mode, we show how merging to instability occurs at all values of ϵ, though for small rotation (small ϵ) a very large α is required before

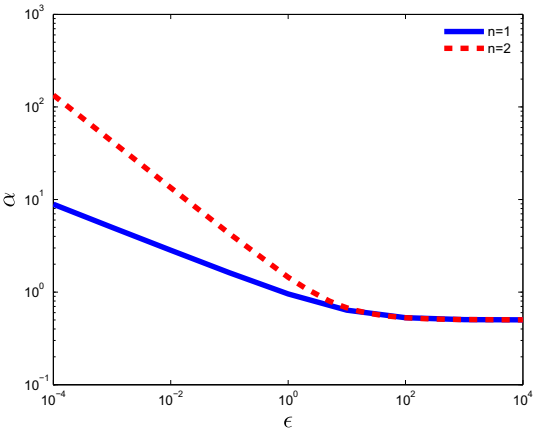

Figure 7. Domain of instability in the $\epsilon - \alpha$ plane. The instability occurs for parameter values above the lines.

instability onsets. Even for large ϵ, it is necessary to have $\alpha > 0.5$ for instability to occur. Figure 7 shows the domain of instability as a function of ϵ and α for the $m = 1$ mode both for $n = 1$ and the more stable $n = 2$ solutions. For small ϵ the critical α for instability appears to scale as $\epsilon^{-1/4}$ in the $n = 1$ case and $\epsilon^{-1/2}$ in the $n \geq 2$ cases.

This instability can be related to the current driven instabilities of Tayler (1973), Tayler (1980) and Pitts and Tayler (1985) who determine the conditions under which a toroidal magnetic field can become unstable to non-axisymmetric disturbances, both in cylindrical and spherical geometries; see also the extensive discussion in Spruit (1999). For these current-driven instabilities the instability draws its energy from the imposed current via the magnetic curvature force. The role of the magnetic field in this case is therefore that it acts as an energy source (with a strong magnetic field being required for the instability to proceed). For these current-driven instabilities the role of rotation is simply to mediate the rate at which energy can be extracted from the mean field. This type of instability should be distinguished from a different class of instabilities that emerge in the presence of both differential rotation and current (see e.g. Gilman and Fox 1997, Gilman and Dikpati (2002), Cally (2003), Cally *et al.* (2008), Hollerbach and Cally (2009)). These *joint instabilities* occur for relatively weak magnetic fields (such as those that may occur in the stable layers of planets and stars) in differentially rotating layers. For these systems the axisymmetric differential rotation and magnetic field, which in isolation would be linearly stable, are together jointly unstable. Here the toroidal magnetic field acts as a conduit to allow the extraction of energy from the differential rotation – though some energy may also be extracted from the current.

This new instability can also be compared with previously known $m = 1$ instabilities in related geophysical problems. Malkus (1967) found an $m = 1$ instability using the same magnetic field as us, $\boldsymbol{B} = B_0 \sin\theta \hat{\boldsymbol{e}}_\phi$. However, in his problem there was no stable stratification, he considered homogeneous rotating fluid in a full sphere. Interestingly, he found a criterion for instability equivalent in our notation to $\alpha > 0.5$. It can be seen from Figure 7 that in the limit $\epsilon \to \infty$ his criterion reduces to ours. This is consistent with the fact that the limit $\epsilon \to \infty$ corresponds to the effect of gravity dropping out of

our problem, which is equivalent to the buoyancy frequency being small compared to the rotation frequency. Diffusive $m = 1$ instabilities have also been found in spherical models. Roberts and Loper (1979) also considered the Malkus field with homogeneous fluid in cylindrical and spherical containers and found that the $m = 1$ modes could become destabilised when Ohmic diffusion is added. Sharif and Jones (2005) considered the fully two-dimensional problem in a spherical shell, which corresponds to very large buoyancy frequency, $\epsilon \to 0$. They considered the case with a basic state zonal flow and a magnetic field, but they found an $m = 1$ instability in the presence of ohmic diffusion even with zero zonal flow, but no instability without magnetic diffusion in this case. They had a slightly more complicated basic state magnetic field, but their result is consistent with ours, because with no magnetic diffusion and small ϵ our critical α for instability goes to infinity.

Figure 6(a) and (b) show some very remarkable features. The westward propagating magnetic Rossby waves all pass through $\alpha = 0.5$, $\lambda = -m/2$ exactly. The fast magnetic Rossby waves are westward propagating super-Alfvénic waves at small α, that is the modulus of their phase speed, $|\lambda/m| > \alpha$, so the wave speed exceeds the Alfvén speed. However, as α increases, they become sub-Alfvénic. Inspection of (16) shows that at transition between the two regimes to avoid singularity we must have both

$$\lambda^2 - \alpha^2 m^2 = 0, \quad \text{and} \quad \lambda + 2m\alpha^2 = 0 \tag{30a,b}$$

$$\Longrightarrow \quad \alpha = 0.5 \quad \text{and} \quad \lambda = -0.5m \tag{30c,d}$$

so transition can only occur at $\alpha = 0.5$ whatever the value of ϵ. So all the fast magnetic Rossby waves have frequency $-m/2$ at $\alpha = 0.5$, whatever ϵ, so all the curves in Figure 6(b) pass through this point. An asymptotic analysis near $\alpha = 0.5$ is given in Section 6.2.2, showing that near the Alfvénic point the solutions are spherical harmonics.

Another interesting feature of Figure 6(b) is that for the $m = 1$ eastward propagating Rossby waves, there is a point where the frequency is zero, i.e. they travel eastwards for α below a critical value and westward above it. This means there is a linear stationary solution which is an equilibrium between the Lorentz, Coriolis and Buoyancy forces.

5.3. Fast magnetic Rossby waves

Figure 8 shows the westward propagating fast magnetic Rossby waves at various α and ϵ. Figure 8(a) and (b) show the mixed Rossby-gravity mode, which is the fastest sinuous mode, $m = n = 1$ in the notation of (22), for a small value of $\alpha = 0.1$. The frequencies of the plotted modes are given in Table 3. We see that at large ϵ, the fast magnetic Rossby mode is equatorially trapped, and an asymptotic analysis is given in Section 6.2.1, but it becomes delocalised as $\alpha \to 0.5$. In the neighbourhood of $\alpha = 0.5$, the asymptotic theory of Section 6.2.2 shows that the solutions are spherical harmonics. This can be seen in Figure 8(c) and (d), which are for $\alpha = 0.49$. Even the $\epsilon = 100$ case shows very little equatorial trapping, and the frequencies are all very close to $\lambda = -0.5$. In Table 4 the frequencies of the $m = 1$, $n = 2$ varicose magnetic Rossby wave are given. This mode is a full Rossby mode rather than a mixed Rossby-gravity mode; at large ϵ and small α the frequency follows the asymptotic behaviour of $\nu = 1$ in (22).

The $m = 1$ case is exceptional, because of the appearance of unstable modes beyond $\alpha = 0.5$, so as α is increased it is replaced by unstable modes. It is still possible to trace

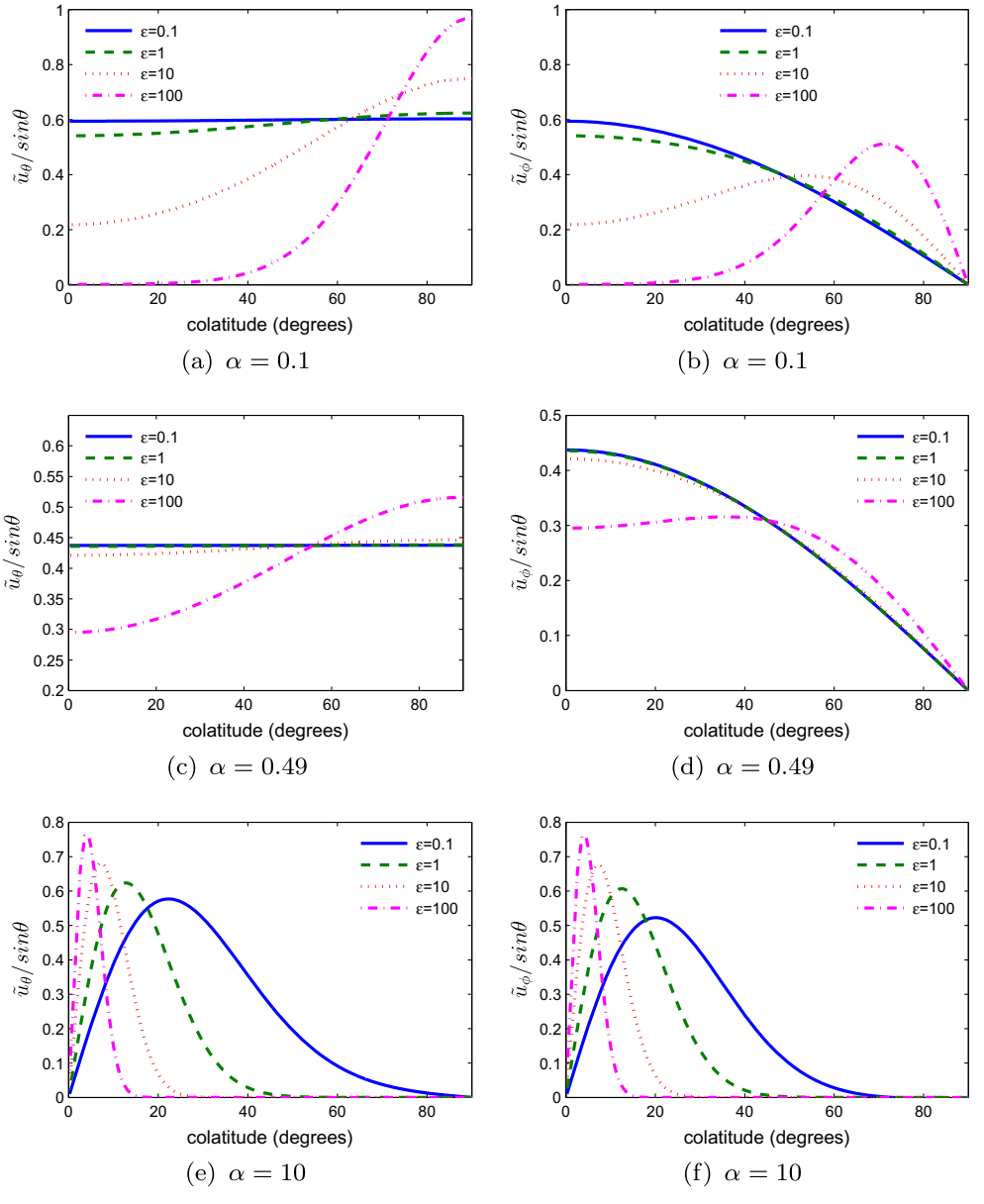

Figure 8. Northward and azimuthal velocities against co-latitude for different values of ϵ and α. These are westward fast magnetic Rossby waves. (a–d) are for $N = 50$, $m = 1$ and $n = 1$, the fastest sinuous mode, which is the mixed Rossby-gravity mode. (a) is $\tilde{u}_\theta / \sin\theta$ and (b) is $\tilde{u}_\phi / \sin\theta$ with $\alpha = 0.1$. The larger ϵ values show equatorial trapping. (c) and (d) are at $\alpha = 0.49$ close to the Alfvénic transition point. (e) and (f) are $m = 2$ $n = 2$ modes for $\alpha = 10$, into the polar trapping regime. The eastward slow magnetic Rossby waves have very similar at this large value of α.

the higher m modes which are still wave-like, but at large α the unstable modes may well change the basic state significantly. However, in Figure 8(e) and (f) we show $m = 2$, $n = 2$ varicose modes at large α. The frequencies of these modes can be found in Table 5. We see that the frequencies increase with α, and the modes become trapped at the poles.

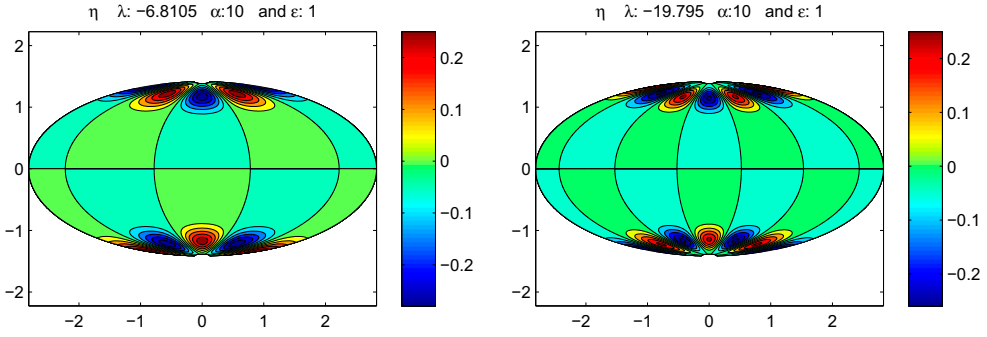

(a) $m = 2$ (b) $m = 3$

Figure 9. Contour plots of the scaled height η for fast magnetic Rossby waves. These illustrate the polar trapping of the Rossby waves at large α. The fastest sinuous mode is shown for (a) $m = 2$, (b) $m = 3$.

Table 3. Eigenvalues λ for the fast magnetic Rossby wave for different values of α and ϵ and with $m = n = 1$. This is the fastest sinuous mode, the mixed Rossby-gravity mode: waves travelling westward. The modes become complex (unstable) at larger values of α.

α	10^{-3}	10^{-2}	10^{-1}	1	10^{1}	10^{2}	10^{3}
$\epsilon = 0.01$	−0.4999	−0.4999	−0.4999	−0.4989	−0.301 – 3.19i	−0.482 – 92.67i	−0.498 – 992.90i
$\epsilon = 0.1$	−0.4988	−0.4988	−0.4989	−0.4883	−0.442 –7.48i	−0.494 – 97.73i	−0.499 – 997.76i
$\epsilon = 1$	−0.4880	−0.4880	−0.4889	−0.294 – 0.12i	−0.482 – 9.25i	−0.498 – 99.29i	−0.500 – 999.29i
$\epsilon = 10$	−0.4140	−0.4141	−0.4202	−0.435 – 0.60i	−0.494 – 9.76i	−0.499 – 99.77i	−0.500 – 999.75i
$\epsilon = 100$	−0.2710	−0.2711	−0.2877	−0.480 – 0.79i	−0.498 – 9.92i	−0.500 – 99.91i	−0.500 – 999.81i

Table 4. Eigenvalues λ for the fast magnetic Rossby waves for different values of α and ϵ, and with $m = 1, n = 2$. Second lowest (varicose) mode: waves travelling westward.

α	10^{-3}	10^{-2}	10^{-1}	1	10^{1}	10^{2}	10^{3}
$\epsilon = 0.01$	− − 0.1665	−0.1669	−0.1999	−0.9034	−5.297	−0.482–92.67i	−0.498–992.90i
$\epsilon = 0.1$	− − 0.1652	−0.1656	−0.1987	−0.8971	−0.443– 7.47i	−0.494 –97.74i	−0.499–997.76i
$\epsilon = 1$	− − 0.1530	−0.1534	−0.1886	−0.8086	−0.482–9.25i	−0.498–99.29i	−0.500 – 999.29i
$\epsilon = 10$	− − 0.0950	−0.0956	−0.1408	−0.437–0.60i	−0.494–9.76i	−0.499 – 99.77i	−0.500 – 999.75i
$\epsilon = 100$	− − 0.033	−0.0346	−0.1054	−0.480 – 0.79i	−0.498 – 9.92i	−0.500 – 99.91i	−0.500 – 999.81i
$\epsilon = 1000$	− − 0.0106	−0.0145	−0.1006	−0.494 – 0.84i	−0.499–9.97i	−0.500 – 99.93i	−0.500 – 999.82i

Table 5. Eigenvalues for the fast magnetic Rossby waves for different values of α and ϵ, $n = 2$ and $m = 2$: waves travelling westward.

α	10^{-3}	10^{-2}	10^{-1}	1	10^{1}	10^{2}	10^{3}
$\epsilon = 0.01$	−0.3333	−0.3341	−0.4000	−1.8080	−15.9209	−63.655	−200.50
$\epsilon = 0.1$	−0.3323	−0.3338	−0.3997	−1.8066	−11.5124	−36.058	−112.97
$\epsilon = 1$	−0.3299	−0.3307	−0.3971	−1.7906	−6.81047	−20.504	****
$\epsilon = 10$	−0.3056	−0.3065	−0.3771	−1.5864	−4.0822	−11.757	****
$\epsilon = 100$	−0.2300	−0.2312	−0.3189	−1.2615	−2.5584	****	****

An asymptotic theory is possible, see Section 6.2.4. Polar trapping occurs for modes with $m \geq 2$ as $\alpha\epsilon^{1/2} \to \infty$ provided the waves are sub-Alfvénic. This means that the fast westward waves are polar trapped for any $\alpha > 0.5$ if ϵ is sufficiently large. In Figure 9 we

Table 6. Eigenvalues for different values of α and ϵ, with $m = 1$, and $n = 1$, the anomalous westward slow magnetic Rossby mode.

α	10^{-2}	10^{-1}	1	10^{1}	10^{2}	10^{3}
$\epsilon = 0.01$	****	-2.000×10^{-7}	-2.005×10^{-3}	$-0.301 + 3.19i$	$-0.482 + 92.67i$	$-0.498 + 992.90i$
$\epsilon = 0.1$	****	-2.000×10^{-6}	-0.02053	$-0.442 + 7.48i$	$-0.494 + 97.73$	$-0.499 + 997.76i$
$\epsilon = 1$	****	-2.000×10^{-5}	$-0.294 + 0.12i$	$-0.482 + 9.25i$	$-0.498 + 99.29i$	$-0.500 + 999.29i$
$\epsilon = 10$	-2.000×10^{-8}	-0.000197	$-0.435 + 0.60i$	$-0.494 + 9.76i$	$-0.499 + 99.77i$	$-0.500 + 999.75i$
$\epsilon = 100$	-2.000×10^{-7}	-0.00172	$-0.480 + 0.79i$	$-0.498 + 9.92i$	$-0.500 + 99.91i$	$-0.500 + 999.81i$

Table 7. Eigenvalues for different values of α and ϵ, with $n = 2$, and $m = 1$. Slow magnetic Rossby modes: waves travelling eastward.

α	10^{-3}	10^{-2}	10^{-1}	1	10^{1}	10^{2}	10^{3}
$\epsilon = 0.01$	4×10^{-6}	0.000399	0.033322	0.73319	4.7293	-0.482+92.67i	-0.498+992.90i
$\epsilon = 0.1$	4×10^{-6}	0.000399	0.033222	0.69392	-0.443+7.47i	-0.494+97.74i	-0.499+997.76i
$\epsilon = 1$	4×10^{-6}	0.000399	0.032244	0.28655	-0.482 + 9.25i	-0.498 + 99.29i	-0.500 + 999.29i
$\epsilon = 10$	4×10^{-6}	0.000397	0.024642	-0.437+ 0.60i	-0.494 + 9.76i	-0.499 + 99.77i	-0.500 + 999.75i
$\epsilon = 100$	4×10^{-6}	0.00038	0.004171	-0.4940 + 0.84i	-0.499 + 9.97i	-0.500 + 99.93i	-0.500+ 999.82i

Table 8. Eigenvalues for different values of α and ϵ, with $m = 2$, and $n = 2$, an eastward slow magnetic Rossby mode. Modes all real in this $m = 2$ case.

α	10^{-3}	10^{-2}	10^{-1}	1	10^{1}	10^{2}	10^{3}
$\epsilon = 0.01$	7.9998×10^{-6}	0.0007981	0.06667	1.4738	15.480	62.705	199.50
$\epsilon = 0.1$	7.9998×10^{-6}	0.0007981	0.06664	1.4649	10.677	35.073	111.97
$\epsilon = 1$	7.9998×10^{-6}	0.0007980	0.06641	1.3557	5.8606	19.508	****
$\epsilon = 10$	7.9998×10^{-6}	0.0007976	0.06407	0.7645	3.0980	10.759	****
$\epsilon = 100$	7.9994×10^{-6}	0.0007936	0.04446	0.3153	1.5634	****	****

show the scaled surface displacement η for two polar trapped modes, $m = 2$ and $m = 3$, illustrating the nature of these modes.

5.4. Slow magnetic Rossby waves

At small α, the smallest frequencies correspond to slow magnetic Rossby waves generally propagating eastward. The only exception is the anomalous $m = n = 1$ mode, which travels westward as seen in Table 6, and for which the eigenfunctions are shown in Figure 10(a) and (b). Note that $\tilde{b}_\theta / \sin\theta$ and $\tilde{b}_\phi / \sin\theta$ are shown, because the energy of a slow magnetic Rossby mode is mainly magnetic, rather than kinetic or potential energy. Note that in Table 6 at larger α all the modes are complex, corresponding to instability.

The frequencies of the slow magnetic Rossby waves (except at $m = n = 1$) can all be approximated at small ϵ and α by (29) with the plus sign. The anomalous $m = n = 1$ mode gives $\lambda = 0$ in this approximation; the asymptotics of this anomalous mode are given in Appendix A. In Table 7 the eigenvalues for the eastward propagating $m = 1$, $n = 2$ slow magnetic Rossby wave are given. The eigenfunctions for this varicose mode are shown for $\alpha = 0.1$ in Figure 10(c) and (d). The mode $m = 1$, $n = 2$ also becomes unstable at larger α. Although in table 7 we see eastward propagation for low α for this mode, we know

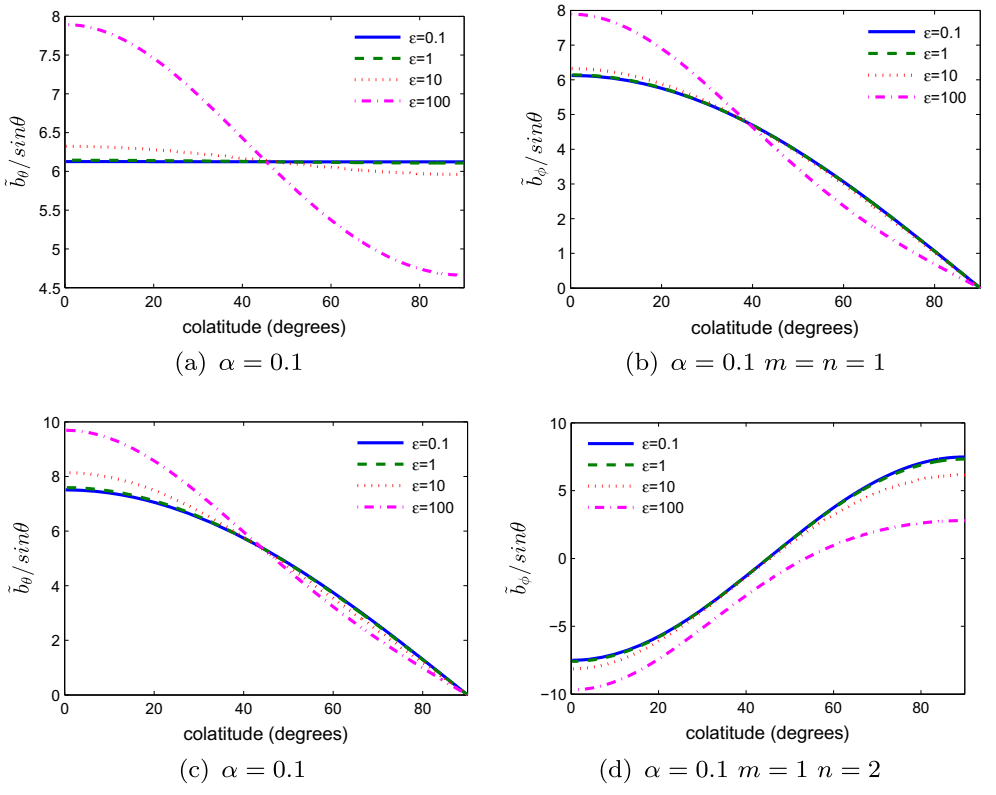

Figure 10. Meridional and azimuthal magnetic fields for slow magnetic Rossby waves. (a) and (b) are for $\alpha = 0.1$, $m = 1$ and is the anomalous westward propagating slow sinuous mode. (c) and (d) are for the eastward propagating $n = 2$, $m = 1$ varicose mode.

from Figure 6(b) that the mode becomes westward shortly before it goes unstable, and the frequency of the unstable modes is not far from -0.5. The asymptotics of this mode at large α is given in Section 6.2.4.

The $m = 2$ mode never becomes unstable even at large α, see Table 8. At large α the mode become trapped at the poles, and behaves very similarly to the fast magnetic Rossby mode shown in Figure 9, though it travels eastward rather than westward. The asymptotics at large α for $m \geq 3$ are also given in Section 6.2.4. They are always sub-Alfvénic. The $m = 2$ mode is again somewhat anomalous, and is dealt with in Appendix B.

5.5. Unstable Rossby waves

The eigenfunctions associated with the unstable $m = 1$ modes are shown in Figure 10. At moderate ϵ and α they form the usual sequence of alternating sinuous and varicose modes, filling the whole spherical surface, but these unstable modes also become polar trapped at large α or ϵ, and can be analysed asymptotically in these limits, see Section 6.2.4 (see Figures 11 and 12).

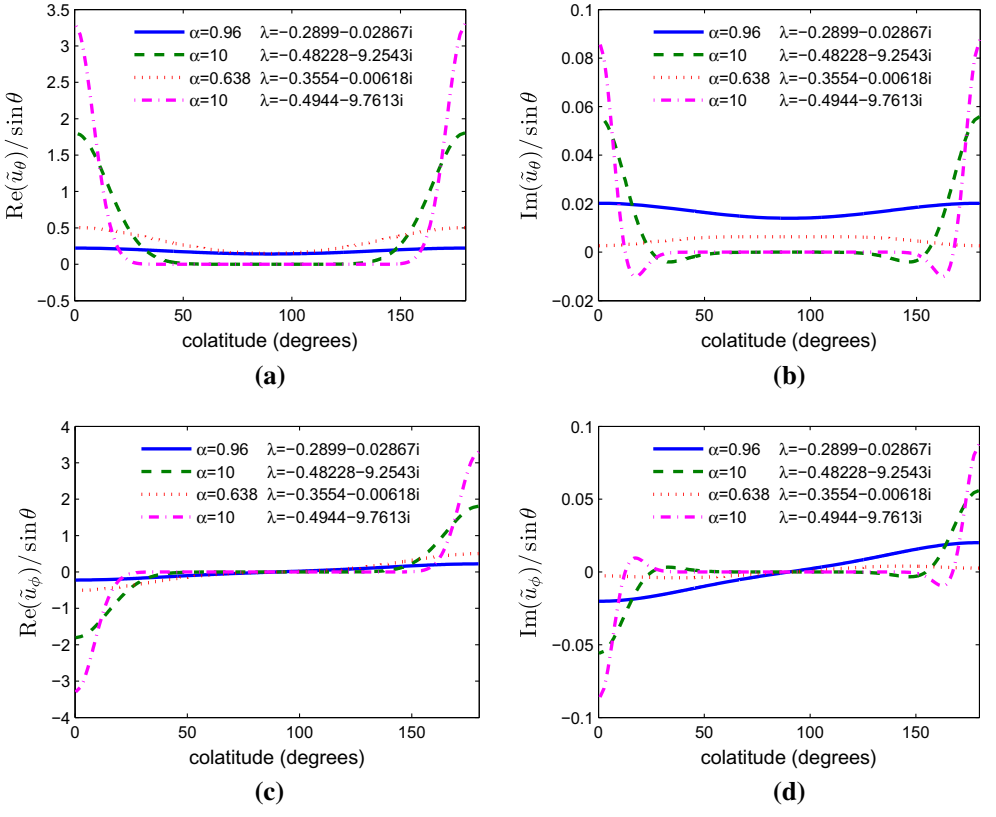

Figure 11. Eigenfunctions for unstable modes. $m = 1$. (a) shows the real part of $\tilde{u}_\theta / \sin\theta$ and (b) shows its imaginary part. Note the co-latitude goes from north to south pole. (c) and (d) are the real and imaginary parts of $\tilde{u}_\phi / \sin\theta$. The blue solid curve at $\alpha = 0.96$ has $\epsilon = 1$ and the red dotted curve at $\alpha = 0.638$ has $\epsilon = 10$. Both these cases are close to marginal stability. The green dashed and magenta dash-dot curves are for $\alpha = 10$, $\epsilon = 1$ and $\epsilon = 10$ respectively and are strongly supercritical polar trapped modes.

5.6. Kelvin waves

For the non-magnetic case, Longuet-Higgins found just one eastward propagating wave corresponding to the Kelvin mode, and he established that at small ϵ, the Kelvin mode corresponds to the first eastward propagating gravity wave, $(n - m = 0)$, with dispersion relation (19a,b). When ϵ is large, the waves are equatorially trapped and the dispersion relation becomes (23). He also noted that when ϵ is large the northward velocity $\tilde{u}_\theta$ is much smaller than the azimuthal velocity.

When a toroidal magnetic field is introduced into the system, Kelvin waves become trapped at the equator for both large α and large ϵ, as can be seen in Figures 13) and (14). From the numerical results, we note that on increasing ϵ or α the northward velocity goes to zero quickly, which is a useful property of this magneto-Kelvin mode. The original set of equations, when $\tilde{u}_\theta = 0$, reduces to

$$(\lambda + 2m\alpha^2)\mu\tilde{u}_\phi + \lambda(1-\mu^2)\frac{\partial\eta}{\partial\mu} = 0, \tag{31a}$$

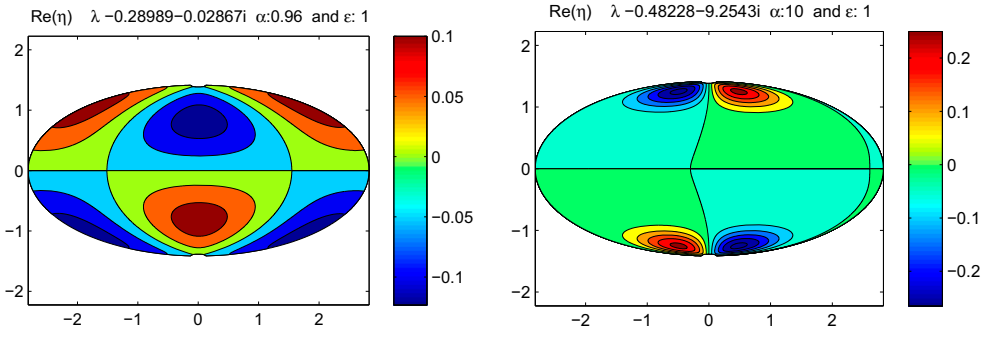

(a) $\alpha = 0.96$, $\epsilon = 1$ (b) $\alpha = 10$, $\epsilon = 1$

Figure 12. Contour plots of the scaled height η for unstable waves. The mode on the left (a) is close to the onset of instability, on the right (b) the mode is strongly unstable and trapped at the poles. Note that the contours of zero η are no longer lines of longitude, but slope on the θ-ϕ surface.

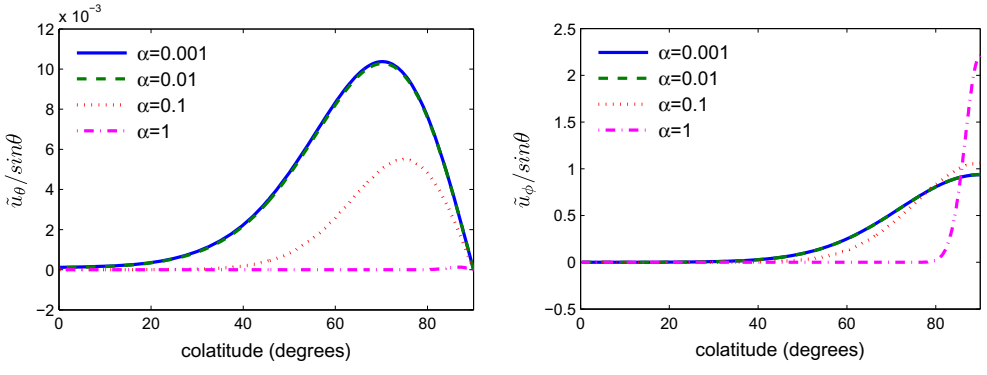

(a) $u_\theta / \sin\theta$ (b) $u_\phi / \sin\theta$

Figure 13. Numerical solution for different values of α for the Magneto Kelvin Mode with $m = 1$, $\epsilon = 100$ and $N = 50$. (a) Northward velocity, (b) Azimuthal velocity.

$$(\lambda^2 - m^2\alpha^2)\tilde{u}_\phi - \lambda m\eta = 0, \tag{31b}$$

$$\lambda\epsilon(1-\mu^2)\eta - m\tilde{u}_\phi = 0. \tag{31c}$$

Eliminating η between (31a) and (31b) gives

$$(1-\mu^2)\frac{\mathrm{d}\tilde{u}_\phi}{\mathrm{d}\mu} + \frac{m(\lambda + 2m\alpha^2)}{(\lambda^2 - m^2\alpha^2)}\mu\tilde{u}_\phi = 0, \tag{32}$$

with solution

$$\tilde{u}_\phi = C_1\left(1-\mu^2\right)^{q/2}, \qquad q = \frac{m(\lambda + 2m\alpha^2)}{(\lambda^2 - m^2\alpha^2)}, \tag{33a,b}$$

where C_1 is a constant associated with the normalisation. When the waves are equatorially trapped, q is large and the solution is close to zero except when μ is small, so using (33a,b) and (31b),

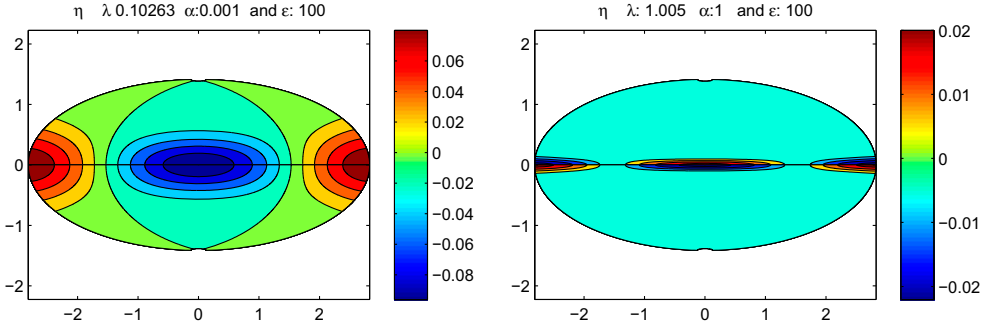

Figure 14. Numerical solution for the scaled height η increasing $\alpha = 0.001$ in (a) and $\alpha = 1$ in (b), for Magneto Kelvin mode with $m = 1, \epsilon = 100$ and $N = 50$.

$$\tilde{u}_\phi \sim C_1\left(1 - \tfrac{1}{2}q\mu^2\right), \qquad \eta \sim C_1 \frac{(\lambda^2 - m^2\alpha^2)}{\lambda m}\left(1 - \tfrac{1}{2}q\mu^2\right). \tag{34a,b}$$

Substituting these expressions for η and $\tilde{u}_\phi$ into Equation (31c), and taking the limit, $1 - \mu^2 \sim 1$ appropriate for equatorially trapped waves, leads to the dispersion relation

$$\lambda^2 - m^2\alpha^2 = \frac{m^2}{\epsilon} \qquad \text{giving} \qquad \lambda = \pm m\sqrt{\frac{1}{\epsilon} + \alpha^2}. \tag{35a,b}$$

Note that if $\alpha = 0$, the dispersion relation coincides with Longuet-Higgins formula for equatorially trapped Kelvin waves. An interesting issue is whether both signs in the dispersion relation give meaningful solutions. When α is small, the negative sign gives $q < 0$ in (33a,b), which does not correspond to an equatorially trapped mode. Longuet-Higgins therefore found only eastward propagating Kelvin waves. In the magnetic case, the situation is different, because provided

$$\alpha > \frac{1}{2}\left(\frac{1}{2} + \sqrt{\frac{1}{4} + \frac{4}{\epsilon}}\right)^{1/2} \tag{36}$$

the negative root gives positive q. Of course, α must exceed this inequality by some margin, as we require q large, not just positive, for trapped waves, but nevertheless this shows that westward propagating Kelvin waves can be found at large α, which is not possible in the nonmagnetic case.

The frequencies for some eastward propagating magneto-Kelvin waves are shown in Table 9. For small α the results are consistent with the Longuet-Higgins nonmagnetic formulae, while for large α the results are in good agreement with (35a,b). The starred entries are when the equatorially trapping is so strong our numerical program could not accurately resolve the solution. As usual, these are precisely the cases where the asymptotic formula (35a,b) becomes very accurate.

In Table 10, some westward propagating magneto-Kelvin waves are shown. Naturally, there are no such waves for small α, and for small ϵ even the $\alpha = 1$ case gives no westward magneto-Kelvin wave. Again, at large α there are resolution problems, but for moderately

Table 9. Numerical results for eigenvalues λ that correspond to the Kelvin mode for $m = 1$. Waves travelling eastward.

α	10^{-3}	10^{-2}	10^{-1}	1	10^{1}	10^{2}	10^{3}
$\epsilon = 0.01$	13.9	13.9	13.9	13.9012	15.2263	100.5000	****
$\epsilon = 0.1$	4.2452	4.2452	4.2453	4.2649	10.4999	100.0500	****
$\epsilon = 1$	1.2307	1.2307	1.2323	1.4782	10.0050	****	****
$\epsilon = 10$	0.34457	0.34468	0.35618	1.0496	10.0050	****	****
$\epsilon = 100$	0.10263	0.10309	0.14257	1.005	****	****	****

Table 10. Numerical results for eigenvalues λ that correspond to the Kelvin mode for $m = 1$. Waves travelling westward.

α	1	10^{1}	10^{2}
$\epsilon = 0.01$	****	−15.3966**	−100.5000
$\epsilon = 0.1$	****	−10.5013	****
$\epsilon = 1$	−1.6888**	−10.050	****
$\epsilon = 10$	−1.0516	−10.0050	****
$\epsilon = 100$	−1.0050	****	****

large α we have good agreement with the predictions of (35a,b) with the negative sign. The starred entries at $\alpha = \epsilon = 1$ and $\alpha = 10, \epsilon = 0.01$ are on the westward propagating Kelvin branch, but because q is not very large at these values, they are not strongly trapped at the equator, so the asymptotic theory does not give accurate frequencies for these two points.

6. Asymptotic theory at large ϵ or large α

An attractive feature of this problem is that many of the key results can be derived using asymptotic theory, which give simple formulae for the eigenvalues in many cases. Here we describe these asymptotic theories. Numerical comparisons between the asymptotics and the numerical results, many of which are remarkably close, are given in Appendix C.

6.1. MIG waves

The asymptotics at large ϵ and α are best dealt with starting from Equation (16). Magneto-inertial gravity waves are trapped near the equator when ϵ is large even if α is small (Longuet-Higgins 1968), and from Figures 4 and 5 we see that even at moderate ϵ MIG waves become trapped as α get large. Also, the fast magnetic Rossby wave can be equatorially trapped at small α and large ϵ, but for these large ϵ waves equatorial trapping is lost as $\alpha \to 0.5$. The slow magnetic Rossby wave is not equatorially trapped. We first treat the equatorially trapped MIG waves,

6.1.1. Equatorially trapped MIG waves

As α increases, the frequency λ increases and for these fast waves $\lambda^2 > m^2\alpha^2$. For waves which are non-zero only near the equator, we can take $\mu = \cos\theta$ to be small. Since μ is small, and either ϵ or α is large the factor $[\epsilon(\lambda^2 - \alpha^2 m^2)(1 - \mu^2) - m^2]$ tends to $\sim \epsilon(\lambda^2 - \alpha^2 m^2)$, and the first derivative term in (16) is negligible.

Then Equation (16) becomes

$$\frac{\mathrm{d}^2\tilde{u}_\theta}{\mathrm{d}\mu^2}+\left[(\lambda^2-\alpha^2m^2)\epsilon-\frac{m(\lambda+2m\alpha^2)}{(\lambda^2-\alpha^2m^2)}\right]\tilde{u}_\theta-\frac{\epsilon(\lambda+2m\alpha^2)^2}{(\lambda^2-\alpha^2m^2)}\mu^2\tilde{u}_\theta=0. \tag{37}$$

We rescale $\mu = s\hat{\mu}$ where the scale factor

$$s=\frac{1}{\sqrt{2}}\left[\frac{(\lambda^2-\alpha^2m^2)}{\epsilon(\lambda+2\alpha^2m)^2}\right]^{1/4}\hat{\mu}, \tag{38}$$

and the rescaled equation becomes

$$\frac{\mathrm{d}^2\tilde{u}_\theta}{\mathrm{d}\hat{\mu}^2}+\frac{1}{2}\left[\frac{(\lambda^2-\alpha^2m^2)}{\epsilon(\lambda+2\alpha^2m)^2}\right]^{1/2}\left[(\lambda^2-\alpha^2m^2)\epsilon-\frac{m(\lambda+2m\alpha^2)}{(\lambda^2-\alpha^2m^2)}\right]\tilde{u}_\theta-\frac{1}{4}\hat{\mu}^2\tilde{u}_\theta=0. \tag{39}$$

This equation is a parabolic cylinder equation, which has solutions which decay as $\hat{\mu}\to\pm\infty$ provided

$$\frac{1}{2}\left[\frac{(\lambda^2-\alpha^2m^2)}{\epsilon(\lambda+2\alpha^2m)^2}\right]^{1/2}\left[(\lambda^2-\alpha^2m^2)\epsilon-\frac{m(\lambda+2m\alpha^2)}{(\lambda^2-\alpha^2m^2)}\right]=\nu+\frac{1}{2}, \tag{40}$$

where $\nu = 0, 1, 2, \ldots$ is a non-negative integer. The regular solution $\tilde{u}_\theta$ for this differential equation is given by $D_\nu(\hat{\mu})$, the parabolic cylinder function (Abramowitz and Stegun 1965). The lowest order solutions are, for $\nu = 0, 1, 2$: $\tilde{u}_\theta = \exp[-(1/4)\hat{\mu}^2]$ (sinuous mode), $\tilde{u}_\theta = \hat{\mu}\exp[-(1/4)\hat{\mu}^2]$ (varicose mode) and $\tilde{u}_\theta = (\hat{\mu}^2-1)\exp[-(1/4)\hat{\mu}^2]$ respectively. Equation (40) can be squared and written as an 8th order polynomial in λ, which can be solved using standard numerical polynomial solvers. However, some care is needed because not every root of the 8th order equation corresponds to an acceptable solution of (39).

For Equation (39) to be a valid approximation, it is clearly necessary that the scale factor s be small. In the limit $\alpha\to 0$ we know that at large ϵ the gravity waves have $\lambda\sim\pm(2\nu+1)^{1//2}\epsilon^{-1/4}$, so s is indeed small. Also, we note that at $\epsilon\sim O(1)$, s becomes small at large α.

We now look at the asymptotic behaviour of (40) first in the limit $\epsilon\to\infty$ with α small. We recover the (Longuet-Higgins, 1968) result, that

$$\lambda=\pm\frac{(2\nu+1)^{1/2}}{\epsilon^{1/4}}+\frac{m}{\epsilon^{1/2}(4\nu+2)}, \tag{41}$$

the plus sign being for the eastward propagating MIG waves and the minus sign for the westward propagating waves. Note that from (24) the $n = 2$ eastward mode connects with $\nu = 0$, so $\nu = 0$ in (41) to get approximations to the table 1 results, while from (24) the $n = 2$ westward mode connects with $\nu = 2$, so in (41) we need $\nu = 2$ as well as the minus sign to get agreement with table 2 in this limit. Note also that because this expansion is in powers of $\epsilon^{1/4}$, these approximations are not very accurate unless ϵ is very large.

We now consider the limit of (40) in which ϵ remains of order unity as $\alpha\to\infty$. From the results in Tables 1 and 2 we see that $|\lambda|$ exceeds $m\alpha$ in this limit but only by a relatively

small amount at large α. We therefore let $\lambda = \delta + m\alpha$ and expand in powers of the small parameters δ/λ and $1/\alpha$, to obtain the dispersion relation at large α and $\epsilon \sim \mathrm{O}(1)$

$$\lambda = \pm\left[m\alpha + (2\nu+1)^{2/3}\left(\frac{\alpha}{2m\epsilon}\right)^{1/3} + \frac{(2m)^{1/3}}{(2\nu+1)^{2/3}\alpha^{1/3}\epsilon^{2/3}}\left(\frac{1}{3} - \frac{(2\nu+1)^2}{4m^2}\right)\right] + \frac{(2\nu+1)^{2/3}}{3(2m\epsilon\alpha^2)^{1/3}}, \tag{42}$$

which is accurate to $\mathrm{O}(\alpha^{-2/3})$, terms of order α^{-1} and smaller being omitted. Here the plus sign refers to waves propagating eastwards, the minus sign to waves propagating westwards. In Appendix C we see that (42) gives accurate estimates of λ at large α.

6.2. Fast and slow magnetic Rossby waves

We now consider the asymptotics of the fast and slow magnetic Rossby waves. We start by considering small α and monitor developments as α gradually increases. At small ϵ, the fast magnetic Rossby waves are simply spherical harmonics, but at large ϵ the fast magnetic Rossby waves are equatorially trapped (Longuet-Higgins 1968), and so the same theory based on (39) can be applied, and asymptotic approximations obtained from (40).

6.2.1. Equatorially trapped fast magnetic Rossby waves

Equatorially trapped fast westward magnetic Rossby waves are found when ϵ is large and $\alpha < 0.5$. Since ϵ is large, the analysis of (37)–(40) is valid here, but now on the left-hand side of (40)

$$(\lambda^2 - \alpha^2 m^2)\epsilon \ll -\frac{m(\lambda + 2m\alpha^2)}{(\lambda^2 - \alpha^2 m^2)}. \tag{43}$$

Note that as the waves are westward and super-Alfvénic ($\lambda < -m\alpha$) for $\alpha < 0.5$, the factor $\lambda + 2m\alpha^2$ is negative, while $\lambda^2 - \alpha^2 m^2 > 0$. The dispersion relation (40) therefore becomes

$$\lambda^2 = \alpha^2 m^2 + \frac{m^2}{(2\nu+1)^2\epsilon}, \qquad \text{so} \qquad \lambda = -m\alpha\left(1 + \frac{1}{(2\nu+1)^2\epsilon\alpha^2}\right)^{1/2}. \tag{44}$$

It can now be verified that at large ϵ (43) holds in the range $0 < \alpha < 0.5$ provided α is not too close to 0.5. In the limit $\alpha \to 0$ this dispersion relation reduces to the Longuet-Higgins result (22), as expected. Recall that the integer $\nu \geq 1$ for a valid solution. When $0.5 > \alpha \gg \epsilon^{-1/2}$, a binomial expansion is valid, and

$$\lambda \sim -m\alpha - \frac{m}{2\epsilon\alpha(2\nu+1)^2}, \tag{45}$$

which gives good agreement with the numerical results at large ϵ and α in this range. The factor $\lambda + 2m\alpha^2 \sim -2m\alpha(0.5 - \alpha)$, so it is clear that as $\alpha \to 0.5$ the magnetic Rossby waves, unlike the MIG waves, become delocalised, no longer trapped at the equator. The fast magnetic Rossby waves are westward propagating super-Alfvénic waves at small α, that is the modulus of their phase speed, $|\lambda/m| > \alpha$, so the wave speed exceeds the Alfvén speed. However, as α increases, they become sub-Alfvénic. From (30a,b) we know that the transition can only occur at $\alpha = 0.5$ whatever the value of ϵ. So all the fast magnetic

Rossby waves have frequency $-m/2$ at $\alpha = 0.5$. We now detail the asymptotic analysis in the neighbourhood of $\alpha = 0.5$.

6.2.2. Fast magnetic Rossby waves near $\alpha = 0.5$

Let $\alpha = 0.5 + \hat{\alpha}$, $\lambda = -m/2 + \delta$ where $\hat{\alpha}$ is small and $\delta \sim \mathrm{O}(\hat{\alpha})$ and insert into (16), noting that $\epsilon(\lambda^2 - \alpha^2 m^2)(1-\mu^2) \ll m^2$, the ODE becomes

$$(1-\mu^2)\frac{\mathrm{d}^2\tilde{u}_\theta}{\mathrm{d}\mu^2} - 2\mu\frac{\mathrm{d}\tilde{u}_\theta}{\mathrm{d}\mu} + \left[\frac{\delta + 2m\hat{\alpha}}{\delta + m\hat{\alpha}} - \frac{m^2}{1-\mu^2}\right]\tilde{u}_\theta = 0, \tag{46}$$

which is just the associated Legendre equation, so the solutions are spherical harmonics of degree n, where

$$n(n+1) = \frac{\delta + 2m\hat{\alpha}}{\delta + m\hat{\alpha}} \qquad \Longrightarrow \qquad \delta = m\hat{\alpha}\frac{[2 - n(n+1)]}{n(n+1) - 1} \tag{47a,b}$$

giving a simple formula for the frequency which agrees excellently with our numerical solutions of the full Equation (16). This solution is valid for all ϵ and $m \neq 0$, showing that at large ϵ the fast magnetic Rossby waves delocalise from their equatorially trapped state at $\alpha \approx 0.5$, the opposite behaviour from the MIG waves, which concentrate further at the equator as α increases. Once the fast magnetic Rossby waves have become sub-Alfvénic another asymptotic regime develops as α increases beyond 0.5, and the waves become trapped at the poles. However, before developing this theory we consider the slow magnetic Rossby waves.

6.2.3. Slow magnetic Rossby waves at small α

These waves have a frequency which goes to zero as $\alpha \to 0$ and so do not appear in the non-magnetic theory. The normal behaviour of these modes is that $\lambda \sim \mathrm{O}(\alpha^2)$ as $\alpha \to 0$ and we again have that in (16) $\epsilon(\lambda^2 - \alpha^2 m^2)(1-\mu^2) \ll m^2$ leading to a great simplification. Noting that now $\lambda^2 \ll m^2\alpha^2$, and writing $\lambda = \hat{\lambda}\alpha^2$ equation becomes

$$(1-\mu^2)\frac{\mathrm{d}^2\tilde{u}_\theta}{\mathrm{d}\mu^2} - 2\mu\frac{\mathrm{d}\tilde{u}_\theta}{\mathrm{d}\mu} + \left[2 + \frac{\hat{\lambda}}{m} - \frac{m^2}{1-\mu^2}\right]\tilde{u}_\theta = 0, \tag{48}$$

which is again the associated Legendre equation, but this time with

$$\hat{\lambda} = m\big[n(n+1) - 2\big], \qquad \text{for positive integer } n, \tag{49}$$

from which we deduce that slow magnetic Rossby waves travel eastwards at small α. Clearly the case $n = 1$, which implies $m = 1$, is exceptional, and in Appendix A we show that this mode has the very slow frequency $\lambda = -\epsilon\alpha^4/5$ at small α. Remarkably, this is the only westward propagating slow magnetic Rossby wave that occurs at small α. We also note that since the frequency vanishes at small ϵ, it was not picked up in the small ϵ analysis of Zaqarashvili *et al.* (2007).

We now consider what happens to slow magnetic Rossby modes as α increases, and the behaviour of fast magnetic Rossby waves beyond $\alpha = 0.5$ where they become sub-Alfvénic. All the Rossby modes remain sub-Alfvénic as α increases beyond 0.5. As we

saw in Section 5, the $m = 1$ slow and fast magnetic Rossby waves collide at a particular value of α and beyond this value there are unstable complex modes. For $m \geq 2$ the slow and fast magnetic Rossby waves remain distinct, and correspond to purely wavelike solutions. An asymptotic theory at large α is possible, as the waves become trapped at the poles. Interestingly, this theory can be developed for the $m = 1$ unstable modes as well as the wave like solutions. The case $m = 2$ is exceptional, and is dealt with in Appendix B.

6.2.4. Magnetic Rossby waves at large α

We start with the $m = 1$ case, because this establishes the existence of unstable modes in this problem independently of any numerical analysis. We seek solutions that are trapped at the pole, and since the behaviour is essentially identical at both poles we focus on $\mu = 1$, the north pole. We assume α is large and ϵ is order unity. A double limit analysis is possible, but for simplicity we keep to $\epsilon \sim \mathrm{O}(1)$. The numerics suggested that the eigenvalues have the form

$$\lambda = -\tfrac{1}{2} + \mathrm{i}(\alpha - \kappa), \tag{50}$$

where κ is a constant of order unity to be determined. This is the growing mode; the decaying mode $\lambda = -\frac{1}{2} - \mathrm{i}(\alpha - \kappa)$ behaves very similarly and can be treated in the same way. There are two relevant scalings of (16), the first being

$$\text{(i)} \qquad \mu = 1 - \frac{\gamma_1 \hat{\mu}}{\alpha}, \tag{51}$$

where γ_1 is a constant of order unity, to be determined later. $\hat{\mu}$ is an order one variable, and we seek solutions with $\tilde{u}_\theta \to 0$ as $\hat{\mu} \to \infty$. Because α is large these correspond to solutions with significant amplitude only near the pole. We now insert (50) and (51) into (16) and retain only the terms of order α, which give the leading order equation. At first sight it appears that the terms with factors $\epsilon(\lambda^2 - \alpha^2 m^2)$ and $-\epsilon\mu^2(\lambda + 2m\alpha^2)^2/(\lambda^2 - \alpha^2 m^2)$ are of order α^2; however, because μ is close to 1, these order α^2 terms cancel out. The condition for this to happen in the sub-Alfvénic case is that

$$\lambda^2 - \alpha^2 m^2 = -(\lambda + 2m\alpha^2) \qquad \Longrightarrow \qquad \lambda = -\tfrac{1}{2} \pm \sqrt{\tfrac{1}{4} + \alpha^2 m(m-2)} \tag{52a,b}$$

which, if $m = 1$, gives $\lambda \approx \pm \mathrm{i}\alpha$ as expected, see (50), but gives only real solutions for all other m. This type of growing mode solution can only exist if $m = 1$. Taking account of this cancellation of the $\mathrm{O}(\alpha^2)$ terms, and making the convenient choice $\gamma_1 = (8\epsilon)^{-1/2}$, (16) reduces to Whittaker's equation

$$\frac{\mathrm{d}^2 \tilde{u}_\theta}{\mathrm{d}\hat{\mu}^2} + \left[-\frac{1}{4} + \sqrt{\frac{\epsilon}{2}} \frac{\kappa}{\hat{\mu}} + \frac{1}{4\hat{\mu}^2} \right] \tilde{u}_\theta = 0, \tag{53}$$

Abramowitz and Stegun (1965). Provided that

$$\kappa = \left(n + \tfrac{1}{2}\right)\sqrt{2/\epsilon} \tag{54a}$$

for some non-negative integer n, (53) has solution

$$\tilde{u}_\theta = \mathrm{e}^{-\hat{\mu}/2}\hat{\mu}^{1/2}\mathrm{L}_n(\hat{\mu}), \tag{54b}$$

which decays as $\hat{\mu} \to \infty$, and has $\tilde{u}_\theta \to \hat{\mu}^{1/2}$ as $\hat{\mu} \to 0$. $\mathrm{L}_n(\hat{\mu})$ are the Laguerre polynomials of degree n, so $\mathrm{L}_0 = 1$ and $\mathrm{L}_1 = 1 - x$. The predicted values of κ agree well with the numerical solution, indicating that (54a) is the desired solution with eigenvalue

$$\lambda = -\tfrac{1}{2} + \mathrm{i}\big[(\alpha - (n + \tfrac{1}{2})\sqrt{2/\epsilon}\,\big]. \tag{55}$$

However, this is not quite conclusive, as in the course of this asymptotic analysis the term $\epsilon(\lambda^2 - \alpha^2 m^2)(1 - \mu^2)$ has been assumed of order α, which led to the first derivative term being considered asymptotically negligible. However, this quantity tends to zero as $\hat{\mu} \to 0$, so the neglect of this term cannot be justified over the whole domain of interest. We therefore consider a second scaling

$$\text{(ii)} \qquad \mu = 1 - \frac{\gamma_2 \tilde{\mu}}{\alpha^2}, \tag{56}$$

which removes this singularity as now $\epsilon(\lambda^2 - \alpha^2 m^2)(1 - \mu^2)$ has the same order as the m^2 term. Making the convenient choice $\gamma_2 = (1/4)\epsilon$, we obtain

$$\tilde{\mu}\frac{\mathrm{d}^2\tilde{u}_\theta}{\mathrm{d}\tilde{\mu}^2} + \frac{1}{1+\tilde{\mu}}\frac{\mathrm{d}\tilde{u}_\theta}{\mathrm{d}\mu} - \frac{\tilde{u}_\theta}{4\tilde{\mu}} + \frac{2\epsilon\gamma_2\tilde{u}_\theta}{1+\tilde{\mu}} = 0. \tag{57}$$

Remarkably, this unpromising looking Equation 57 has the simple exact general solution

$$\tilde{u}_\theta = C_1\tilde{\mu}^{1/2} + C_2\frac{\tilde{\mu}\ln\tilde{\mu} - 1}{\tilde{\mu}^{1/2}}. \tag{58}$$

To obtain a solution that decays as $\tilde{\mu} \to 0$ we must choose $C_2 = 0$. The solution $\tilde{\mu}^{1/2}$ is then valid right through this transition region of thickness $\mathrm{O}(1/\alpha^2)$ and matches correctly as $\tilde{\mu} \to \infty$ onto the Whittaker equation solution as $\hat{\mu} \to 0$, showing that the leading order asymptotic expansions match correctly.

The stable case for $m \geq 3$ behaves similarly, though $m = 2$ is stable but somewhat exceptional (see Appendix B). We now have

$$\lambda = \alpha\sqrt{m(m-2)} + \kappa_+ \tag{59}$$

as the leading order approximation for the eastward propagating mode. The analysis is very similar to the unstable $m = 1$ case above, the Whittaker equation now being

$$\frac{\mathrm{d}^2\tilde{u}_\theta}{\mathrm{d}\hat{\mu}^2} + \left[-\frac{1}{4} + \sqrt{\frac{\epsilon(m-2)}{8}}\frac{(2\kappa_+ + 1)}{\hat{\mu}} + \left(\frac{m}{2} - \frac{m^2}{4}\right)\frac{1}{\hat{\mu}^2}\right]\tilde{u}_\theta = 0. \tag{60}$$

Provided that

$$\kappa_+ = -\frac{1}{2} + \left(n + \frac{m}{2}\right)\sqrt{\frac{2}{\epsilon(m-2)}}, \tag{61a}$$

for some non-negative integer n, (60) has the solution

$$\tilde{u}_\theta = \mathrm{e}^{-\hat{\mu}/2}\hat{\mu}^{m/2}\mathrm{L}_n^{(m-1)}(\hat{\mu}); \tag{61b}$$

the lowest mode being $n = 0$. The generalised Laguerre polynomials $\mathrm{L}_n^{(s)}(\hat{\mu})$ are related to the usual Laguerre polynomials (Abramowitz and Stegun, 1965) by

$$\mathrm{L}_n^{(s)}(\hat{\mu}) = (-1)^s \frac{\mathrm{d}^s}{\mathrm{d}\hat{\mu}^s}\mathrm{L}_{n+s}(\hat{\mu}). \tag{62}$$

These solutions decay as $\hat{\mu} \to \infty$, and have $\tilde{u}_\theta \to \hat{\mu}^{m/2}$ as $\hat{\mu} \to 0$. For the westward propagating fast magnetic Rossby wave, we write

$$\lambda = -\alpha\sqrt{m(m-2)} - \kappa_- \tag{63}$$

and the Whittaker equation is the same except the factor $(2\kappa_+ + 1)$ is replaced by $(2\kappa_- - 1)$ so the condition for κ_- is

$$\kappa_- = +\frac{1}{2} + \left(n + \frac{m}{2}\right)\sqrt{\frac{2}{\epsilon(m-2)}}, \tag{64}$$

so the magnitude of the frequency of the 'fast' westward propagating Rossby wave is one greater than that of the 'slow' eastward propagating Rossby wave, though at large α the form of the waves becomes very similar.

We have here considered ϵ to be of order unity, but actually the parameter that needs to be large for polar trapping is $\alpha\sqrt{\epsilon}$. To get to the polar trapped limit for the Rossby waves, they must be sub-Alfvénic, so for the westward wave we must have $\alpha > 0.5$, but provided this holds, the wave becomes trapped at the poles for large ϵ as well as for large α. For the eastward slow Rossby wave, the mode can be trapped at the pole even for small α provided ϵ is large enough.

7. Summary and conclusions

Using numerical and asymptotic methods a fairly complete picture of the waves and instabilities in this MHD shallow water model has been obtained, extending the work of Longuet-Higgins (1968). These results are specific to the case where the basic state magnetic field is azimuthal and has the simple $\sin\theta$ form, and variations in the basic state height profile are ignored. This case may not be a realistic representation of the complicated scenario in planets and stars, where the magnetic fields have a complicated morphology and zonal flows, thermal wind shears may be important and isosurfaces of pressure may not be spherical. However it does provide a platform from which to explore more realistic field configurations.

The waves can be divided into MIG waves, Kelvin waves, fast magnetic Rossby waves and slow magnetic Rossby waves. With no magnetic field, the fast MIG waves are inertial-gravity waves which become equatorially trapped in the rapid rotation limit of large ϵ. With magnetic field, the MIG waves become equatorially trapped as α increases even at moderate ϵ. These waves, which can travel eastward or westward, are always super-Alfvénic, that is

their phase speed exceeds the Alfvén speed. However, at large α the phase speed is close to the Alfvén speed so these waves turn into equatorially trapped Alfvén waves when the field becomes strong.

The Rossby waves found in the non-magnetic case turn into westward fast magnetic Rossby waves in the MHD case. They are initially super-Alfvénic, but become sub-Alfvénic at $\alpha = 0.5$ and remain sub-Alfvénic at higher α. At large α they become trapped at the poles, and can be asymptotically described using the Whittaker equation, similar to the behaviour in the radial field model of Heng and Spitkovsky (2009). The slow magnetic Rossby waves are an entirely distinct branch, with no counterpart in the non-magnetic problem. Mostly they propagate eastward at small α, but there is one anomalous very slow $m = 1$ mode which travels westward. As α is increased, the other $m = 1$ waves go through a zero frequency and then travel westward, ultimately colliding with the fast magnetic Rossby wave to give complex unstable waves. For $m \geq 2$ the slow magnetic Rossby waves continue going eastward as α increases and become trapped at the pole. These waves are also governed by a Whittaker equation in the large α limit.

The eastward propagating Kelvin wave in the non-magnetic case continues to travel eastward as α is increased, becoming more equatorially trapped. These waves keep their 'Kelvin' character in that the fluid motion is mainly east–west with very little latitudinal flow. The new feature introduced by magnetic field is that at sufficiently strong α a westward Kelvin mode, with very little latitudinal motion, comes into existence.

In planetary applications the results on wave propagation are of interest: for example in the adiabatically stratified outer core of the Earth slow magnetic Rossby waves travel westward, but in the stably stratified layer they travel eastward, apart from the anomalous $m = 1$ mode. This change in the direction of propagation could therefore potentially be used to determine the location of any wave modes that might be detectable in the geomagnetic field. We note that signals in the secular variation of the geomagnetic field have recently been interpreted as magnetic Rossby waves propagating in a stable layer just below the CMB, Chulliat *et al.* (2015). We stress again that, before applying this work to geomagnetic problems, it would be helpful to repeat the analysis for a more realistic basic state magnetic field, but the present work gives clues to the likely outcome of such studies.

For sufficiently large magnetic field ($\alpha > 0.5$), we found that the $m = 1$ slow and fast magnetic Rossby wave branches coalesce when the magnetic field is sufficiently strong, leading to the onset of unstable growing modes. This is a current driven instability of the type previously studied by Tayler (1973, 1980) and Pitts and Tayler (1985) in the astrophysical context and Malkus (1967) and others in the geophysical context. Interestingly, as the field strength is increased, the unstable eigenfunctions become trapped at the poles and are well described by an asymptotic model. We stress here that it is likely that in stars and planets the presence of differential rotation may lead to the presence of joint instabilities of the type introduced by Gilman and Fox (1997) for field strengths that are significantly lower than those required for current driven instabilities. Moreover the simple nature of the basic state means that as the magnetic field is increased the nature of the assumptions included in the force balance will play a more important role in determining the stability of the field (as noted by Pitts and Tayler (1985)). We are currently investigating this.

There are a number of ways in which the study of waves in spherical shallow water MHD could be extended. More realistic azimuthal fields could be considered, and magnetic diffusion could be added, which would be relevant to the Earth's core. It would also be of

interest to explore the effects of a radial field. There is a difficulty here to be overcome, which is that if there is radial field at the interface, magnetic energy can be carried out of the layer. The Gilman azimuthal field model avoids this difficulty because the interface remains a field line.

We conclude by issuing a note of caution for the direct application of our results to stars and planets. Here we echo the sentiments of Pitts and Tayler (1985) who state '...because we have been discussing model problems and because in several cases we have only been able to provide a very approximate discussion, the results which we have obtained are suggestive rather than rigorous'. Clearly the direct application of such results to a star or planet must take into account the assumptions that have gone into formulating the model. The model presented here is convenient, as it allows the analytic derivation of many results in a number of asymptotic limits. We are currently investigating the robustness of these results to changes in the nature of the model, such as varying the ingredients in the latitudinal force balance.

Disclosure statement

No potential conflict of interest was reported by the authors.

Funding

This work was supported by the Universidad Nacional de Costa Rica [grant number JB-C0596-2013].

References

Abramowitz, M., and Stegun, I.A., 1965. *Handbook of mathematical functions: with formulas, graphs, and mathematical tables*, Vol. 55, Dover Publications Inc.

Acheson, D.J. and Hide, R., 1973. Hydromagnetics of rotating fluids. *Reports on Progress in Physics*, 36, 159–221.

Braginsky, S.I., 1998. Magnetic Rossby waves in the stratified ocean of the core, and topographic core-mantle coupling. *Earth Planets Space*, 50, 641–649.

Cally, P.S., 2003. Three-dimensional magneto-shear instabilities in the solar tachocline. *Monthly Notices of the Royal Astronomical Society*, 339, 957–972.

Cally, P.S., Dikpati, M. and Gilman, P.A., 2008. Three-dimensional magneto-shear instabilities in the solar tachocline - II. Axisymmetric case. *Monthly Notices of the Royal Astronomical Society*, 391, 891–900.

Cho, J.Y.K., 2008. Atmospheric dynamics of tidally synchronized extrasolar planets. *Philosophical Transactions of the Royal Society A*, 366, 4477–4488.

Christensen-Dalsgaard, J., Thompson, M.J., 2007. Observational results and issues concerning the tachocline. *In* D.W. Hughes, R. Rosner, and N.O. Weiss, eds. *The solar tachocline*, 53.

Chulliat, A., Alken, P. and Maus, S., 2015. Fast equatorial waves propagating at the top of the Earth's core. *Geophysical Research Letters*, 42, 3321–3329.

Dikpati, M. and Gilman, P.A., 2001. Prolateness of the slar tachocline inferred from latitudinal force balance in a magnetohydrodynamic shallow-water model. *Astrophysical Journal*, 552, 348–353.

Dikpati, M., Gilman, P.A. and Rempel, M., 2003. Stability analysis of tachocline latitudinal differential rotation and coexisting toroidal band using a shallow-water mdel. *Astrophysical Journal*, 596, 680–697.

Finlay, C., Dumberry, M., Chulliat, A. and Pais, M., 2010. Short timescale core dynamics: theory and observations. *Space Science Reviews*, 155, 177–218.

Gill, A.E., 1982. *Atmosphere-ocean dynamics*, Vol. 30, Academic Press.

Gilman, P.A. and Dikpati, M., 2002. Analysis of instability of latitudinal differential rotation and toroidal field in the solar tachocline using a magnetohydrodynamic shallow-water model. I. Instability for broad toroidal field profiles. *Astrophysical Journal*, 576, 1031–1047.
Gilman, P.A. and Fox, P.A., 1997. Joint instability of latitudinal differential rotation and toroidal magnetic fields below the solar convection zone. *Astrophysical Journal*, 484, 439–454.
Gilman, P.A., 2000. Magnetohydrodynamic "Shallow Water" equations for the solar tachocline. *Astrophysical Journal Letters*, 544, L79.
Grazzini, F. and Vitart, F., 2015. Atmospheric predictability and Rossby wave packets. *Quarterly Journal of the Royal Meteorological Society*, 141, 2793–2802.
Helffrich, G. and Kaneshima, S., 2010. Outer-core compositional stratification from observed core wave speed profiles. *Nature*, 468, 807–810.
Heng, K. and Spitkovsky, A., 2009. Magnetohydrodynamic shallow water waves: linear analysis. *Astrophysical Journal*, 703, 1819–1831.
Hide, R., 1969. On hydromagnetic waves in a stratified rotating incompressible fluid. *Journal of Fluid Mechanics*, 39, 283–287.
Hollerbach, R. and Cally, P.S., 2009. Nonlinear evolution of axisymmetric twisted flux tubes in the solar tachocline. *Solar Physics*, 260, 251–260.
Hughes, D.W., 2007. Magnetic buoyancy instabilities in the tachocline. *In* D.W. Hughes, R. Rosner, and N.O. Weiss, eds. *The solar tachocline*, 275.
Koskinen, T.T., Cho, J.Y.K., Achilleos, N. and Aylward, A.D., 2010. Ionization of extrasolar giant planet atmospheres. *Astrophysical Journal*, 722, 178–187.
Koskinen, T.T., Yelle, R.V., Lavvas, P. and Cho, Y.-K.J., 2014. Electrodynamics on extrasolar giant planets. *Astrophysical Journal*, 796, 16.
Legarreta, J., Barrado-Izagirre, N., García-Melendo, E., Sánchez-Lavega, A. and Gómez-Forrellad, J.M., 2016. A large active wave trapped in Jupiter's equator. *Astrophysics and Astronomy*, 586, A154.
Longuet-Higgins, M.S., 1968. The eigenfunctions of Laplace's tidal equations over a sphere. *Philosophical Transactions of the Royal Society A*, 262, 511–607.
MacGregor, K.B. and Rogers, T.M., 2011. Reflection and ducting of gravity waves inside the Sun. *Solar Physics*, 270, 417–436.
Malkus, W.V.R., 1967. Hydromagnetic planetary waves. *Journal of Fluid Mechanics*, 28, 793–802.
Mathis, S. and de Brye, N., 2011. Low-frequency internal waves in magnetized rotating stellar radiation zones. I. Wave structure modification by a toroidal field. *Astronomy and Astrophysics*, 526, A65.
Mcintosh, S.W., Cramer, W.J., Pichardo, M. and Leamon, R.J., in press. The Detection of Rossby-Like Waves On The Sun. *Nature Astronomy*.
Miesch, M.S., 2005. Large-scale dynamics of the convection zone and tachocline. *Living Reviews in Solar Physics*, 2.
Pitts, E. and Tayler, R.J., 1985. The adiabatic stability of stars containing magnetic fields. IV - The influence of rotation. *Monthly Notices of the Royal Astronomical Society*, 216, 139–154.
Rashid, F.Q., Jones, C.A. and Tobias, S.M., 2008. Hydrodynamic instabilities in the solar tachocline. *Astronomy and Astrophysics*, 488, 819–827.
Rempel, M., Schüssler, M. and Tóth, G., 2000. Storage of magnetic flux at the bottom of the solar convection zone. *Astronomy and Astrophysics*, 363, 789–799.
Roberts, P. and Loper, D., 1979. On the diffusive instability of some simple steady magnetohydrodynamic flows. *Journal of Fluid Mechanics*, 90, 641–668.
Schecter, D.A., Boyd, J.F. and Gilman, P.A., 2001. "Shallow-water" magnetohydrodynamic waves in the solar tachocline. *Astrophysical Journal*, 551, L185–L188.
Sharif, B. and Jones, C., 2005. Rotational and magnetic instability in the diffusive tachocline. *Geophysical & Astrophysical Fluid Dynamics*, 99, 493–511.
Spiegel, E.A. and Zahn, J.P., 1992. The solar tachocline. *Astronomy and Astrophysics*, 265, 106–114.
Spruit, H.C., 1999. Differential rotation and magnetic fields in stellar interiors. *Astronomy and Astrophysics*, 349, 189–202.

Tayler, R.J., 1973. The adiabatic stability of stars containing magnetic fields-I. Toroidal fields. *Monthly Notices of the Royal Astronomical Society*, 161, 365.
Tayler, R.J., 1980. The adiabatic stability of stars containing magnetic fields. IV - Mixed poloidal and toroidal fields. *Monthly Notices of the Royal Astronomical Society*, 191, 151–163.
Tobias, S.M., 2015. The solar tachocline: Formation, stability and its role in the solar dynamo. *In* A.M. Soward, C.A. Jones, D.W. Hughes, and N.O. Weiss, eds. *Fluid dynamics and dynamos in astrophysics and geophysics*, 193.
Vallis, G.K., 2006. *Atmospheric and oceanic fluid dynamics*, Cambridge University Press.
Zaqarashvili, T., Oliver, R. and Ballester, J., 2009. Global shallow water magnetohydrodynamic waves in the solar tachocline. *Astrophysical Journal Letters*, 691, L41.
Zaqarashvili, T., Oliver, R., Ballester, J. and Shergelashvili, B., 2007. Rossby waves in "shallow water" magnetohydrodynamics. *Astronomy and Astrophysics*, 470, 815–820.

Appendix A. The anomalous slow magnetic Rossby mode $n = m = 1$

In Section 5.2 we showed that in the limit $\alpha \to 0$ the slow magnetic Rossby waves have frequency given by

$$\lambda = m\alpha^2\big(n(n+1) - 2\big), \tag{A.1}$$

for integer n and m with $n \geq m$, see (29), where $\tilde{u}_\theta = \mathrm{P}_n^m(\cos\theta)$. This predicts eastward propagating waves, but it clearly breaks down when $n = 1$. In this case, the numerical results suggested a formula of the form

$$\lambda = \hat{\lambda}\epsilon\alpha^4, \tag{A.2}$$

where $\hat{\lambda}$ is a constant to be determined. In this asymptotic treatment, we are assuming that ϵ remains of order unity as $\alpha \to 0$. Our starting point is Equation (16) with $m = 1$ and (A.2) inserted. Expanding in powers of α^2 and discarding terms of $\mathrm{O}(\alpha^4)$ and higher we obtain

$$(1-\mu^2)\frac{\mathrm{d}^2\tilde{u}_\theta}{\mathrm{d}\mu^2} - 2\mu\frac{\mathrm{d}\tilde{u}_\theta}{\mathrm{d}\mu} + 2\tilde{u}_\theta - \frac{\tilde{u}_\theta}{1-\mu^2} + \epsilon\alpha^2\left[2\mu(1-\mu^2)\frac{\mathrm{d}\tilde{u}_\theta}{\mathrm{d}\mu} + \big(\hat{\lambda} + 8\mu^2 - 1\big)\tilde{u}_\theta\right] = 0. \tag{A.3}$$

The leading order solution is $\tilde{u}_\theta = (1-\mu^2)^{1/2}$ but this does not determine $\hat{\lambda}$. We therefore let $\tilde{u}_\theta = (1-\mu^2)^{1/2} + \epsilon\alpha^2 y$, and obtain equation for y, namely

$$(1-\mu^2)\frac{\mathrm{d}^2 y}{\mathrm{d}\mu^2} - 2\mu\frac{\mathrm{d}y}{\mathrm{d}\mu} + 2y - \frac{y}{1-\mu^2} = (1 - \hat{\lambda} - 6\mu^2)(1-\mu^2)^{1/2}. \tag{A.4}$$

The particular integral which satisfies the boundary conditions is $y = A(1-\mu^2)^{3/2}$, which when inserted into (A.4) gives

$$A(10\mu^2 - 2) = 1 - \hat{\lambda} - 6\mu^2, \qquad \text{leading to} \qquad A = -\frac{3}{5}, \quad \hat{\lambda} = -\frac{1}{5}. \tag{A.5a,b}$$

This value of $\hat{\lambda}$ agrees excellently with our numerical solutions for small values of α. The anomalous slow magnetic Rossby mode therefore travels westward, whereas all other magnetic Rossby waves at small α travel eastward. The leading order solution for this wave is simply $\tilde{u}_\theta = \mathrm{P}_1^1(\cos\theta)$.

Appendix B. Polar trapped Rossby waves at large α with $m = 2$

We now consider an exceptional case arising from the large α theory for the magnetic Rossby waves. Recall that for $m = 1$ unstable modes occur, and for $m \geq 3$ stable waves are found with frequency λ proportional to α. It is clear from (59) that the case $m = 2$ must behave differently, and the numerical results indicate that when $m = 2$ the frequency is real, and increases with α, but more slowly than for $m \geq 3$. Asymptotic analysis suggests that for $m = 2$

$$\lambda = \beta\alpha^{1/2} + \kappa, \tag{B.1}$$

where β and κ are constants to be determined. The two scalings for μ,

$$\text{(i)} \qquad \mu = 1 - \frac{\gamma_1 \hat{\mu}}{\alpha}, \qquad\qquad \text{(ii)} \qquad \mu = 1 - \frac{\gamma_2 \tilde{\mu}}{\alpha^2} \tag{B.2}$$

still hold, and we begin with scaling (i). Inserting (i) and (B.1) into (16) and retaining only the terms of order α and $\alpha^{1/2}$, omitting terms of order unity, we get the leading order equation. As before, the terms with factors $\epsilon(\lambda^2 - \alpha^2 m^2)$ and $-\epsilon\mu^2(\lambda + 2m\alpha^2)^2/(\lambda^2 - \alpha^2 m^2)$ are of order α^2; however, because μ is close to 1, the order α^2 terms cancel out. In this $m = 2$ case, a further cancellation occurs between the terms with factors

$$-\frac{m^2}{1-\mu^2} - \frac{2\epsilon m(\lambda + 2m\alpha^2)\mu^2}{[(\lambda^2 - \alpha^2 m^2)\epsilon(1-\mu^2) - m^2]}$$

which is O(1) rather than the expected O(α). Making the convenient choice $\gamma_1 = (1/4)\epsilon^{1/2}$, we obtain as our leading order equation

$$\frac{\mathrm{d}^2 \tilde{u}_\theta}{\mathrm{d}\hat{\mu}^2} + \left[-\frac{1}{4} + \frac{\beta^2 \epsilon^{1/2}}{4\hat{\mu}} + \frac{\beta \epsilon^{1/2}(1+2\kappa)}{4\alpha^{1/2}\hat{\mu}} \right] \tilde{u}_\theta = 0, \tag{B.3}$$

which is a Whittaker equation (Abramowitz and Stegun, 1965). We remove the $\alpha^{-1/2}$ term by setting $\kappa = -\frac{1}{2}$. Then, provided that

$$\beta^2 = 4(n+1)\big/\epsilon^{1/2}, \tag{B.4a}$$

(B.3) has a solution

$$\tilde{u}_\theta = \mathrm{e}^{-\hat{\mu}/2}\hat{\mu}\mathrm{L}_n^{(1)}(\hat{\mu}), \tag{B.4b}$$

where $\mathrm{L}_n^{(1)}(\hat{\mu})$ is the generalized Laguerre function (see (62). The lowest $n = 0$ mode is $\mathrm{L}_0^{(1)}(\hat{\mu}) = 1$. These solutions decay as $\hat{\mu} \to \infty$ and are proportional to $\hat{\mu}$ as $\hat{\mu} \to 0$. This is consistent with the second scaling (ii), as this gives

$$\tilde{\mu}\frac{\mathrm{d}^2 \tilde{u}_\theta}{\mathrm{d}\tilde{\mu}^2} + \frac{1}{1+\tilde{\mu}}\frac{\mathrm{d}\tilde{u}_\theta}{\mathrm{d}\mu} - \frac{\tilde{u}_\theta}{\tilde{\mu}} + \frac{\tilde{u}_\theta}{1+\tilde{\mu}} = 0, \tag{B.5}$$

when we choose $\gamma_2 = 1/(2\epsilon)$. $\tilde{u}_\theta = \tilde{\mu}$ is an exact solution of this equation, verifying that the solution (B.4a) is uniformly valid. The frequencies of the $m = 2$ magnetic Rossby modes are therefore given by

$$\lambda = \beta\alpha^{1/2} - \frac{1}{2}, \tag{B.6a}$$

where

$$\beta = \pm\frac{2(n+1)^{1/2}}{\epsilon^{1/4}}, \qquad n = 0, 1, 2 \ldots ; \tag{B.6b}$$

the plus and minus signs giving the eastward and westward propagating waves respectively. As with the $m \geq 3$ case, the magnitude of the westward travelling wave is one larger than the magnitude of the eastward propagating wave.

Appendix C. Comparison of asymptotic and numerical results

In Table C1 we compare the results of Tables 1 and 2 with the asymptotic formula (42) for some larger values of α, with $m = 1$. Also shown are the results from solving the 8th order equation derived from squaring (40). Note that the connection for both the eastward and westward waves and the small α, small ϵ theory of (19a,b) is that ν in (42) corresponds to $\nu = n - m - 1$ (unlike the connection in (25)), so that $\nu = 0$ has been used here to compare with both Tables 1 and 2, which have $n = 2$, $m = 1$. Recall that the $m = n$ eastward and westward gravity mode evolves into the magneto-Kelvin modes, which have different asymptotics.

Table C1. Comparison between numerical and asymptotic estimates of the eigenvalues: MIG waves.

α	ϵ	Numerical	Asymptotic (42)	Asymptotic (40)
Eastward propagating waves				
10	0.1	14.357	14.033	13.896
10	1.0	11.839	11.816	11.799
10	10	10.833	10.831	10.828
100	0.1	108.09	108.068	108.047
100	1.0	103.72	103.719	103.716
1000	0.01	1037.1	1037.079	1037.055
1000	0.1	1017.2	1017.154	1017.152
Westward propagating waves				
10	0.1	−14.102	−13.787	−13.621
10	1.0	−11.719	−11.702	−11.679
10	10	−10.779	−10.778	−10.775
100	0.1	−108.03	−108.016	−107.992
100	1.0	−103.7	−103.694	−103.692
1000	0.01	−1037.1	−1037.054	−1037.031
1000	0.1	−1017.2	−1017.143	−1017.140

Table C2. Comparison between numerical and asymptotic estimates of the eigenvalues: equatorially trapped fast magnetic Rossby waves.

α	ϵ	Numerical	Asymptotic (44)
0.001	10	−0.095	−0.1054
0.001	100	−0.033	−0.0333
0.001	1000	−0.0106	−0.0106
0.01	10	−0.0956	−0.1059
0.01	100	−0.0346	−0.0348
0.01	1000	−0.0145	−0.0145
0.1	10	−0.1408	−0.1453
0.1	100	−0.1054	−0.1054
0.1	1000	−0.1006	−0.1006

Table C3. Comparison between numerical and asymptotic estimates of the eigenvalues: unstable $m = 1$ polar trapped magnetic Rossby waves.

α	ϵ	Numerical	Asymptotic (44)
100	0.01	$-0.482 + 92.67i$	$-0.5 + 92.929i$
100	0.1	$-0.494 + 97.73i$	$-0.5 + 97.764i$
100	1	$-0.498 + 99.29i$	$-0.5 + 99.293i$
100	10	$-0.499 + 99.77i$	$-0.5 + 99.776i$
100	100	$-0.500 + 99.91i$	$-0.5 + 99.929i$
1000	0.01	$-0.498 + 992.90i$	$-0.5 + 992.929i$
1000	0.1	$-0.499 + 997.76i$	$-0.5 + 997.764i$
1000	1	$-0.500 + 999.29i$	$-0.5 + 999.293i$
1000	10	$-0.500 + 999.75i$	$-0.5 + 999.776i$
1000	100	$-0.500 + 999.81i$	$-0.5 + 999.929i$

Table C2 compares the numerical results in Table 4 for equatorially trapped fast magnetic Rossby waves with the asymptotic formula (44). This is comparison is for the varicose $m = 1$, $n = 2$ mode travelling westwards, as do all fast magnetic Rossby modes. We therefore use $\nu = 1$ in formula (44) since the relation $\nu = n - m$ holds for these modes. Recall that equatorial trapping of Rossby waves can only occur for fast magnetic Rossby waves, and then only for $\alpha < 0.5$ at large ϵ. Note

Table C4. Comparison between numerical and asymptotic estimates of the eigenvalues: stable $m = 2$ polar trapped magnetic Rossby waves.

α	ϵ	Numerical westward	Asymptotic westward (B.6a)	Numerical eastward	Asymptotic eastward (B.6a)
100	0.01	−63.65	−63.746	62.71	62.746
100	0.1	−36.06	−36.066	35.07	35.066
100	1	−20.50	−20.500	19.51	19.500
100	10	−11.76	−11.747	10.76	10.747
100	100	−6.919	−6.825	5.919	5.825
1000	0.01	−200.50	−200.50	199.50	119.500
1000	0.1	−112.97	−112.97	111.97	111.968
1000	1	−64.50	−63.746	63.50	62.746

the excellent agreement at the largest values of ϵ, but recall that this asymptotic theory must break down as $\alpha \to 0.5$.

Table C3 compares the numerical results for the unstable polar trapped magnetic Rossby waves in Tables 3, 4, 6 and 7 with the asymptotic results given by (55) with $m = 1$. Recall there is no distinction between slow and fast waves as the two branches collide to give the unstable waves. The eigenvalues come as a complex conjugate pair, here we just give the unstable positive imaginary part case. Generally the agreement is good. At $\alpha = 1000, \epsilon = 100$ the agreement is not as good as might be expected. This is due to difficulty resolving the very thin boundary layers with the numerical code. The asymptotic solution will be more accurate for these parameter values.

Table C4 compares the numerical results for the stable polar trapped magnetic Rossby waves in Tables 5 and 8 which have $m = 2$ and $n = 2$ with the asymptotic results given by (B.6a) with $m = 2$ and $n = 0$. The sinuous $m = 2$ $n = 2$ and varicose $n = 3$ modes both have the same asymptotic structure at large α because the eigenfunctions are tiny in the equatorial regions. In the cases $\alpha = 1000, \epsilon = 1$ and $\alpha = 100, \epsilon = 100$, the thin boundary layer was not fully resolved in the numerical code.